J. Fluid Mech. (1997), *vol.* 352, *pp.* 205–243. Printed in the United Kingdom

Instabilities in a plane channel flow between compliant walls

By CHRISTOPHER DAVIES[1] AND PETER W. CARPENTER[2]

[1] School of Mathematical and Information Sciences, Coventry University, Coventry, CV1 5FB, UK

[2] Department of Engineering, University of Warwick, Coventry, CV4 7AL, UK

(Received 6 June 1996 and in revised form 19 May 1997)

The stability of plane channel flow between compliant walls is investigated for disturbances which have the same symmetry, with respect to the channel centreline, as the Tollmien–Schlichting mode of instability. The interconnected behaviour of flow-induced surface waves and Tollmien–Schlichting waves is examined both by direct numerical solution of the Orr–Sommerfeld equation and by means of an analytic shear layer theory. We show that when the compliant wall properties are selected so as to give a significant stability effect on Tollmien–Schlichting waves, the onset of divergence instability can be severely disrupted. In addition, travelling wave flutter can interact with the Tollmien–Schlichting mode to generate a powerful instability which replaces the flutter instability identified in studies based on a potential mean-flow model. The behaviour found when the mean-flow shear layer is fully accounted for may be traced to singularities in the wave dispersion relation. These singularities can be attributed to solutions which represent Tollmien–Schlichting waves in *rigid*-walled channels. Such singularities will also be found in the dispersion relation for the case of Blasius flow. Thus, similar behaviour can be anticipated for Blasius flow, including the disruption of the onset of divergence instability. As a consequence, it seems likely that previous investigations for Blasius flow will have yielded very conservative estimates for the optimal stabilization that can be achieved for Tollmien–Schlichting waves for the purposes of laminar-flow control.

1. Introduction

The eigenmode spectrum of the coupled Orr–Sommerfeld/compliant-wall problem can be extraordinarily complex. The degree of complexity depends on the type of compliant wall and the precise values of the wall parameters. But, certainly, for compliant walls having a marked effect on laminar–turbulent transition, there is a proliferation of eigenmodes which correspond to genuine physical phenomena. This rich variety of eigenmodes was fully appreciated by Benjamin (1960) in his seminal paper which inaugurated the theoretical study of the effects of wall compliance on hydrodynamic stability. The various associated instabilities have been well documented elsewhere, e.g. see Landahl (1962), Benjamin (1963), Carpenter & Garrad (1985, 1986), Riley, Gad-el-Hak & Metcalfe (1988) and Carpenter (1990). What is, perhaps, still lacking is a clear picture of the interconnections among the various modes. It is the main aim of the present paper to elucidate these interconnections.

It seems to us that two main issues remain obscure. First, there is the question of the connection between the divergence instability and the other instabilities, such as the Tollmien–Schlichting waves and travelling wave flutter. Secondly, it is known that these last two instabilities interact and, under certain circumstances, coalesce to form a powerful instability. Potential-flow theory suggests that divergence and travelling wave flutter can also interact and coalesce to form a powerful flutter-type instability. Most aspects of both these processes remain obscure, however.

Divergence is well known in hydro- and aero-elasticity. Physically it is takes the form of a growing surface wave which is either stationary or travels slowly downstream. It is destabilized when the hydrodynamic pressure forces generated by a surface disturbance exceed the restorative structural forces. A simple potential-flow model was used by Landahl (1962) when he originally identified divergence as an instability of compliant walls. Much work has been done since using similar approaches. Very much less is known about the corresponding eigenmode of the combined Orr–Sommerfeld/compliant-wall system. Carpenter & Morris (1990) located a possible candidate eigenmode which was stable, but no unstable eigenmode was found. There can be no doubt of the physical existence of divergence; it has been observed in experiments, e.g. see Gad-el-Hak, Blackwelder & Riley (1984), and also in numerical simulations, see Lucey, Cafolla & Carpenter (1996). The very recent numerical study of Yeo, Khoo & Zhao (1996) has shed considerable light on this matter in the special case of compliant walls comprising a single viscoelastic layer. They show conclusively that divergence is an absolute instability and, *inter alia*, describe how it is affected by wall damping and variations in Reynolds number. The single viscoelastic layer is rather a special case; for other types of compliant wall outstanding questions still remain concerning the effects of wall damping on divergence and the reliability of estimates of the onset speed based on the potential-flow model.

Modal coalescence between travelling wave flutter and Tollmien–Schlichting instability was first identified by Carpenter, Gaster & Willis (1983). It was also noted in Carpenter & Garrad (1985, 1986). A more extensive study was carried out by Willis (1986). He showed that under certain circumstances the two modes coalesced to form a much more powerful instability. He also established that the group velocity is zero at the point of coalescence which is a necessary but not sufficient condition for the onset of absolute instability. A brief account of Willis' work is given by Carpenter (1990). The transitional mode revealed by the study of Sen & Arora (1988) is probably another manifestation of the same phenomenon. Much about this modal coalescence remains obscure. In particular, its connection or relationship with divergence and the role of damping and other wall parameters need to be explained. Does it replace the interaction and coalescence of travelling wave flutter and divergence found with the potential-flow models? Or, is it a separate and distinct phenomenon?

We have chosen to base the present study on the stability of plane channel flow rather than the Blasius boundary layer. This is because the simple parabolic form of the velocity profile makes it possible to develop a more complete analytical treatment. It is also an advantage that this is a truly parallel flow, thereby removing any possible objection to the validity of the Orr–Sommerfeld equation for linear stability analysis. Our main interest is in the use of wall compliance for laminar-flow control. Channel flows are not of direct interest for this application. Nevertheless, the instabilities of channel flows with compliant boundaries are not without interest in their own right. Apart from possible applications in the process industries, there are many applications in biomechanics. A particular example is to be found in modelling the phenomenon of wheezing exhibited by people suffering from lung or bronchial disorders. In this

connection Grotberg & Davies (1980). Grotberg & Reiss (1984) and Grotberg & Shee (1985) have investigated the stability of uniform flow in a channel with flexible boundaries. A more general review on lung and cardiovascular flows is given by Grotberg (1994). Plane channel flows with compliant boundaries are also used to model the collapse of tubes in other biomechanical applications – see, for example, Luo & Pedley (1996) and the brief review by Kamm & Pedley (1989).

The remainder of the paper is set out in the following way. The previous literature on the effects of wall compliance on channel-flow stability is reviewed in §2. The formulation of and the numerical methods for solving the coupled Orr–Sommerfeld/compliant-wall eigenproblem are presented in §3. Results for the pure Tollmien–Schlichting mode are also given here. The central part of the paper is §4 which is devoted to the flow-induced surface instabilities. The inviscid shear-layer theory is set out in §4.1. Its application in a study of travelling wave flutter is presented in §4.2. Corrections to the inviscid theory to allow for the effects of a viscous wall layer are discussed in §4.3 and full numerical solutions of the Orr–Sommerfeld equation are presented in §4.4. Perhaps the most significant results are to be found in §4.5 where modal coalescence and the onset of divergence instability are examined in some detail. Finally conclusions are given in §5.

2. Earlier work

The first study of the effects of wall compliance on the stability of plane channel flow was undertaken by Hains & Price (1962). They numerically integrated the Orr–Sommerfeld equation in order to substantiate, albeit for a simpler flow, the predictions made earlier by Benjamin (1960) for Tollmien–Schlichting waves in a Blasius boundary layer over a compliant surface. Korotkin (1965) later developed the analytic theory for the compliant channel problem, but formulated the boundary conditions incorrectly.† Green & Ellen (1972) presented numerical results showing that, for sufficiently compliant walls, the neutral stability curve for the Tollmien–Schlichting mode could become deformed so as to include an additional region of instability at higher wavenumbers. Because they failed to identify the mode of instability that is now known as travelling wave flutter, Green & Ellen were unable to give a full account of their numerical results.

Tsvelodub (1977) investigated the stability of plane channel flow between compliant walls modelled as unsupported elastic plates. Ganiev, Ukrainskii & Ustenko (1988) then studied a three-dimensional generalization of the same compliant-wall model. Their numerical results suggest that, when variations in the Reynolds number are attributed to alterations in the fluid viscosity, the onset of Tollmien–Schlichting instability may be determined by three-dimensional disturbances. However, in order to interpret their results, Ganiev *et al.* made use of a Squire transformation (Drazin & Reid 1981), which included a scaling of the non-dimensional wall properties. If the Reynolds number is varied by changing the centreline velocity of the mean flow, then the scaling of the non-dimensional wall properties noted by Ganiev *et al.* is precisely what is needed to ensure that the dimensional wall properties are kept constant. From this it follows that a generalization of Squire's theorem, i.e. that two-dimensional disturbances determine the critical Reynolds number in wall-bounded

† No account was taken of the fact that at the perturbed location of the walls, the mean flow is non-zero. Other studies have shown that the neglect of the associated term in the no-slip condition makes a significant difference to the results obtained: the stabilizing effect of wall compliance on Tollmien–Schlichting waves may even be replaced by destabilization (Tsvelodub 1977).

shear flows, can be made for compliant channels. The validity of Squire's theorem has since been demonstrated by Rotenberry & Saffmann (1990) for channels with compliant walls modelled as spring-backed plates.

A number of investigations have been made of the idealized case of plug flow, i.e. constant-velocity flow, between flexible channel walls (Weaver & Paidoussis 1977; Grotberg & Reiss 1984; Grotberg & Shee 1985). These studies aimed to model physical behaviour, such as that displayed by flows in human lung airways, occurring in circumstances somewhat different from those of present interest. Both linear and nonlinear stability investigations were undertaken, with some emphasis on the latter. Such work has been reviewed by Grotberg (1994). However, it should be mentioned that for all of the studies referred to by Grotberg, the absence of shear in the mean flow precludes the Tollmien–Schlichting instability. In the present investigation we are interested in plane channel flow because it provides a model problem which is simpler than the Blasius boundary layer, but still involves a wall-bounded shear flow in which Tollmien–Schlichting waves can grow, ultimately leading to laminar–turbulent transition. Consistent with this outlook, we will not attempt to give any direct account of applications in fields of interest other than drag reduction and transition delay.

Some recent studies of the stability of plane channel flow between flexible walls have been concerned with nonlinear aspects of the problem. Rotenbery & Saffman (1990) derived a Ginzburg–Landau equation for finite-amplitude disturbances, which they used to show that, in principle, the subcritical bifurcation of the Tollmien–Schlichting instability found in rigid-walled channels could be replaced by a supercritical bifurcation for sufficiently compliant walls. Subsequent study by Rotenberry (1992) suggested that the extent of this effect was so limited that it would not be expected to give rise to any significant qualitative difference between the process of transition in compliant-walled channels and what is found in a rigid-walled channel. Rossi (1991) also derived a Ginzburg–Landau equation for the nonlinear evolution of disturbances in a channel, but for a case with broken symmetry; only one of the channel walls was taken to be compliant, the other being kept rigid. The same configuration was then studied by Ehrenstein & Rossi (1993), adopting a more numerical approach.

In the work of Pierce (1992), plane channel flow between flexible walls provides a model problem to illustrate a general method for deriving the Ginzburg–Landau equation in situations involving interfacial instability. For the particular wall parameters that were selected, the critical Reynolds number was found to be below the rigid-wall value and the nature of the instability remained subcritical.

Rotenberry (1992) and Ehrenstein & Rossi (1993) make use of an exceedingly simple model of the compliant wall, whereby only a spring-like element is retained giving, in effect, a Hooke's Law type of response. The value of such a study as a general guide to the effects of wall compliance on the stability of plane channel flow has been called into question by the recent work of Gajjar & Sibanda (1996). They show that misleading results are obtained when the compliant-wall dynamics are over-simplified. Gajjar & Sibanda base their study on a multideck asymptotic analysis and consider both linear and nonlinear instability. A comprehensive set of results is presented to show the effects on flow stability of varying the various wall parameters. Like Ehrenstein & Rossi they consider the case where only one wall is compliant.

The mechanism for the travelling wave flutter instability in compliant channel flows has been investigated recently by Huang (1996) for varicose modes. Gajjar & Sibanda are also well aware of the existence of other instabilities in addition

to Tollmien–Schlichting waves. But the asymptotic structure on which they base their analysis is appropriate for Tollmien–Schlichting waves rather than flow-induced surface instabilities. Nevertheless, they discuss the other eigenmodes in the light of their results which suggest the existence of a fast, short-wavelength, flutter-type instability for large wall damping. With the exception of Pierce (1992), none of the other nonlinear studies of Tollmien–Schlichting waves reviewed above considered, explicitly, the possibility of other instability modes. This is despite the fact that for the wall parameters and Reynolds numbers considered, for example, by Rotenberry & Saffman (1990), an instability other than a Tollmien–Schlichting wave would almost certainly be dominant. Surely it would be preferable to examine the nonlinear intricacies of the Tollmien–Schlichting instability in a context where it is not likely to be usurped as the route to transition by a flow-induced surface instability. (See Lucey & Carpenter 1995 for evidence of the role of such instabilities in transition.) Accordingly, one possible application of the present work would be as an aid in the choice of wall parameters for studies of nonlinear instability.

Finally, we mention two numerical studies which have been concerned with the stability of plane channel flow when only finite sections of the bounding walls are taken to be compliant. In the first of these studies, by Luo & Pedley (1995), one of the channel walls was modelled to include a length of massless tensioned membrane. Self-excited oscillations were discovered for sufficiently large Reynolds numbers. However, in contrast to the studies discussed previously, the pressure gradient due to the mean flow was fully taken into account. The second such study was conducted by the present authors (Davies & Carpenter 1997), who were interested in assessing the spatial adaptation of Tollmien–Schlichting waves as they pass over the ends of a compliant panel. Attention was confined to linear disturbances with the same symmetry as the Tollmien–Schlichting mode. It was discovered that flow-induced surface waves could be excited at the panel ends by the passage of Tollmien–Schlichting waves. The identification of flow-induced surface waves from the simulation data was facilitated by the theoretical analysis presented below.

3. Orr–Sommerfeld equation for a channel with compliant walls

3.1. *General formulation*

This section outlines the mathematical formulation of the linear stability problem for plane channel flow between compliant walls. For the type of compliant wall considered here, an extension of Squire's theorem can be made, provided the wall properties are non-dimensionalized in an appropriate manner (Rotenberry & Saffman 1990). Thus we may confine attention to two-dimensional disturbances. Basing non-dimensionalization on the undisturbed centreline flow speed and channel half-width, a non-dimensional disturbance streamfunction is introduced in the form

$$\psi(x, y, t) = \phi(y)\mathrm{e}^{\mathrm{i}(\alpha x - \omega t)}, \tag{1}$$

where x is the streamwise direction, y is normal to the walls, ϕ the disturbance profile, and α, ω are the spatial wavenumber and temporal frequency respectively. In general, both α and ω could be complex valued. The two special cases, α real, ω complex and α complex, ω real correspond to temporally and spatially growing waves. For the convective Tollmien–Schlichting instabilities found in flows over rigid walls, spatial growth is usually of most physical interest (Gaster 1965).

Substitution of (1) into the linearized vorticity transport equation for the fluid gives the Orr–Sommerfeld equation for the disturbance profile,

$$(U-c)(\mathrm{D}^2-\alpha^2)\phi - U''\phi = \frac{1}{\mathrm{i}\alpha R}(\mathrm{D}^2-\alpha^2)^2\phi\,, \tag{2}$$

where U is the dimensionless mean velocity profile, R is the Reynolds number and $\mathrm{D} = \mathrm{d}/\mathrm{d}y$. For plane channel flow, with the Reynolds number defined using the dimensional channel half-width and the centreline velocity, the non-dimensionalized mean velocity profile takes the form $U = 1-y^2$. The mean flow is driven by a constant pressure gradient $dP/dx = -2/R$. It is assumed that in the case of a compliant-walled channel, the effect of this pressure gradient on the walls can either be ignored, or balanced by prescribed body forces in each wall. Such an assumption is needed to ensure that there is a solution to the coupled fluid/wall equations with the walls statically located at $y = \pm 1$ when the mean flow is unperturbed. (There are also mean-flow shear stresses $\sigma_{12} = \mp 2/R$ which act at the walls. These have no effect on the wall motion for the types of compliant wall considered below, where the wall model excludes tangential motion.)

The mean flow profile is symmetric about the channel centreline, and the upper and lower channel walls are assumed to have the same compliance. Thus there are two decoupled problems for symmetric and antisymmetric disturbances; we can either take $\phi(y) = \phi(-y)$ or $\phi(y) = -\phi(-y)$. For the case of a rigid-walled channel, the stability characteristics are determined by the symmetric $\phi(y) = \phi(-y)$ disturbances alone (Drazin & Reid 1981). Since the present study is motivated by an interest in the stabilizing effect of wall compliance on Tollmien–Schlichting waves, we will only consider symmetric disturbances. Flow-induced surface instabilities will also be separable into symmetric and antisymmetric modes, but without further study it is not clear which symmetry mode will be the least stable. Consequently, the parity restriction that we will impose on our solutions of the Orr–Sommerfeld equation, whilst affording a useful simplification for the investigation of behaviour that is associated, most directly, with the stabilization of Tollmien–Schlichting waves, may not be justifiable for other applications such as those discussed by Huang (1996).

We will show immediately below that the boundary conditions at the fluid/wall interface take homogeneous form. The Orr–Sommerfeld equation together with these boundary conditions then gives an eigenvalue problem. This yields, in principle, a dispersion relation of the form

$$\mathscr{F}(\alpha, \omega, R) = 0\,. \tag{3}$$

3.2. *Wall model and boundary conditions*

The compliant walls of the channel are modelled as spring-backed plates and are constrained to move only in the vertical direction. Letting asterisks denote dimensional quantities and taking η^* as the vertical displacement of the upper wall from its equilibrium position, the equation of motion of the upper wall can be written as

$$\left(m^*\frac{\partial^2}{\partial t^{*2}} + d^*\frac{\partial}{\partial t^*} + B^*\frac{\partial^4}{\partial x^{*4}} - T^*\frac{\partial^2}{\partial x^{*2}} + K^*\right)\eta^* = p^*(h)\,. \tag{4}$$

The wall parameters are: the plate mass per unit area m^*, the wall damping coefficient d^*, the flexural rigidity of the plate B^*, the longitudinal tension per unit width T^*, and the spring stiffness K^*. The hydrodynamic forcing of the wall is given by the perturbation fluid pressure p^* at the mean wall location $y^* = h$, where h is the

dimensional half-width of the channel. The contribution of the normal viscous stress is ignored since it should be negligible for the large values of the Reynolds number that are of current interest.

Various choices are possible for non-dimensionalizing the wall equations using the dimensional channel half-width h, centreline mean fluid velocity U_m, fluid density ρ, and viscosity v . The choice depends on how the Reynolds number R is varied whilst keeping the dimensional wall properties fixed; we want to be able to interpret results for different R as pertaining to the same physical walls. Holding the half-width h, density ρ, and viscosity v fixed, so that $R = U_m h/v$ is varied only through changes in the centreline velocity U_m, we obtain the following non-dimensionalization of the wall properties:

$$m = \frac{m^*}{\rho h}\,,\ d = \frac{d^* h}{\rho v}\,,\ B = \frac{B^*}{h\rho v^2}\,,\ T = \frac{T^* h}{\rho v^2}\,,\ K = \frac{K^* h^3}{\rho v^2}\,. \tag{5}$$

The wall equation can then be written as

$$\left(m\frac{\partial^2}{\partial t^2} + \frac{d}{R}\frac{\partial}{\partial t} + \frac{1}{R^2}\left(B\frac{\partial^4}{\partial x^4} - T\frac{\partial^2}{\partial x^2} + K\right)\right)\tilde{\eta} = \tilde{p}(1)\,, \tag{6}$$

where $x = x^*/h$, $t = t^* U_m/h$, $\tilde{\eta} = \eta^*/h$, and $\tilde{p} = p^*/\rho U_m^2$. With this particular scheme of non-dimensionalization, the previously mentioned extension of Squire's theorem holds, justifying attention being restricted to two-dimensional disturbances in the fluid.

Assuming a normal mode form for the wall displacement, $\tilde{\eta} = \eta\, \mathrm{e}^{\mathrm{i}(\alpha x - \omega t)}$, the linearized fluid boundary conditions at the upper wall are

$$\mathrm{D}\phi(1) + U'(1)\eta = \alpha\phi(1) - \omega\eta = 0\,. \tag{7}$$

Eliminating η between the two conditions gives

$$\alpha U'(1)\phi(1) + \omega \mathrm{D}\phi(1) = 0\,. \tag{8}$$

Writing the perturbation fluid pressure as $\tilde{p} = p\, \mathrm{e}^{\mathrm{i}(\alpha x - \omega t)}$, the wall equation (6) gives

$$\left(-\left(m\omega^2 + \mathrm{i}\frac{1}{R}\omega d\right) + \frac{1}{R^2}(B\alpha^4 + T\alpha^2 + K)\right)\eta = p(1)\,. \tag{9}$$

On eliminating η, using the second condition stated in (7), we obtain

$$\alpha\phi(1) - \mathrm{i}Y(\alpha,\omega)\, p(1) = 0\,, \tag{10}$$

where the wall admittance

$$Y(\alpha,\omega) = \mathrm{i}\omega\left(m\omega^2 + \frac{1}{R}\mathrm{i}d\omega - \frac{1}{R^2}(B\alpha^4 + T\alpha^2 + K)\right)^{-1} \tag{11}$$

is the ratio of the wall velocity to the perturbation fluid pressure at the wall. When the disturbance profile is symmetric, the pressure profile p is antisymmetric, and so the y-momentum equation for the fluid can be integrated across the channel to give

$$p(1) = -\alpha\int_0^1 \left((\alpha U - \omega)\phi - \frac{\mathrm{i}\alpha^2}{R}\phi\right)\mathrm{d}y - \frac{\mathrm{i}\alpha}{R}\mathrm{D}\phi(1)\,. \tag{12}$$

The magnitude of the final term in the above expression is half that of the normal viscous stress acting at the walls. Consistent with the previously made assumption that the fluid stresses driving the wall motion may be approximated using the pressure

alone, this term can be neglected. Similarly, the other term in (12) that involves the factor $1/R$ may be dispensed with. Thus we can choose to calculate the pressure using the approximate expression

$$p(1) = -\alpha \int_0^1 (\alpha U - \omega)\, \phi \, \mathrm{d}y \,. \tag{13}$$

Substitution into the boundary condition (10) then gives a constraint written entirely in terms of the disturbance amplitude ϕ. This constraint and the relation (8) then provide the boundary conditions for the solution of the Orr–Sommerfeld equation.

3.3. *Discretization of the Orr–Sommerfeld equation*

The Orr–Sommerfeld equation is solved numerically using a Chebyshev spectral method (Canuto *et al.* 1988). The disturbance profile ϕ is approximated as a finite series of even Chebyshev polynomials,

$$\phi(y) = \frac{c_1}{2} + \sum_{k=2}^{N} c_k \, T_{2(k-1)}(y) \tag{14}$$

which ensures that ϕ is symmetric about the channel centreline. Before discretization, the Orr–Sommerfeld equation is integrated indefinitely four times to give (for symmetric ϕ)

$$\omega \iint \phi - \alpha \iint U\phi + 2\alpha \iiint U'\phi - \alpha^2 \omega \iiiint \phi + \alpha^3 \iiiint U\phi + \frac{1}{\mathrm{i}R}\left(\phi - 2\alpha^2 \iint \phi + \alpha^4 \iiiint \phi\right) + b_1 + b_2 y^2 = 0 \,, \tag{15}$$

where $\iint \phi$ is shorthand for $\int_0^y \int_0^{y'} \phi(y'')\, \mathrm{d}y''\, \mathrm{d}y'$ etc., and b_1, b_2 are integration constants. This procedure is adopted because the integral operators take a more convenient form than the corresponding differential operators, when they are applied to the Chebyshev expansion for ϕ. The matrix forms of the operators appearing in (15) are specified in the appendix of Bridges & Morris (1984).

The Chebyshev expansion for ϕ is substituted into the left-hand side of the integrated Orr–Sommerfeld equation. The first N coefficients of the resultant Chebyshev series are then set equal to zero, giving N equations for the $N + 2$ unknowns $b_1, b_2, c_1, \ldots, c_N$. There is no need to calculate the integration constants b_1, b_2. Since they only appear in the two equations obtained by setting coefficients of T_0, T_2 to zero, we may replace these equations by two constraints derived from the boundary conditions at the upper wall. In such a manner, we can obtain a system of N equations for the N unknown Chebyshev coefficients $c_1, \ldots, c_N$. (Further details of the procedures involved may be found in Davies 1995.) The discretized Orr–Sommerfeld equation, incorporating the imposed symmetry and upper-wall boundary conditions, can then be cast in the form

$$\left(\sum_{i=0}^{4} \alpha^i \boldsymbol{L}_i\right) \boldsymbol{c} = 0 \tag{16}$$

where $\boldsymbol{c} = (c_1, \ldots, c_N)^T$ is the vector formed by the Chebyshev coefficients of ϕ and the $N \times N$ matrices $\boldsymbol{L}_i$ are independent of α. To obtain a non-trivial solution of (16),

α must satisfy the condition

$$\det\left(\sum_{i=0}^{4}\alpha^{i}\boldsymbol{L}_{i}\right)=0\,. \tag{17}$$

Equation (17) gives a numerical approximation to the dispersion relation (3), obtained from the Chebyshev discretization. The form of (16) is different from that usually found in matrix eigenvalue problems: the eigenvalue α appears to the fourth power rather than linearly as in the standard problem. Consequently, specialized techniques are needed for its solution. The particular numerical methods adopted were taken from the work of Bridges & Morris (1984), to which reference should be made for further details.

3.4. *Preliminary numerical results*

The numerical scheme was checked against previous work. For the case of a rigid-walled channel, the numerically determined eigenvalues agreed exactly with results obtained by Bridges & Morris (1984). For the compliant-walled case, the largest set of results that can be compared directly with results from the present study is included in the work of Green & Ellen (1972), who considered channels with walls modelled as tensioned membranes. In a more recent investigation, Rotenberry (1992) formulated the problem for the same wall model as is used in current work, but only gave results from the numerical solution of the Orr–Sommerfeld equation for a limited range of wall parameters. Good agreement was obtained between results determined using the present numerical methods and those given in the two earlier studies. For instance, points on the neutral stability curves given by Rotenberry could be reproduced. These curves show the stabilization of Tollmien–Schlichting waves as the wall compliance is increased, for the simplistic situation where the wall motion is governed by a form of Hooke's law, i.e. the only non-zero wall parameter is the spring stiffness.

Figure 1 shows neutral stability curves associated with the Tollmien–Schlichting instability, for the case of channels whose walls are modelled as untensioned spring-backed plates with no internal damping. Such a wall model was used by Carpenter & Garrad (1985) in their investigation of the stability of Blasius flow over Kramer-type compliant surfaces.† It can be seen from figure 1 that the effect of increasing wall compliance is to shrink the neutral stability curve, causing it to close into a single loop which then vanishes for sufficiently low values of the wall stiffness parameters B and K. Unlike the situation for Blasius flow, the neutral stability loop does not appear to break into two pieces; there is no remnant of the rigid-wall curve for higher Reynolds numbers. This qualitative difference must be due to the different non-dimensionalizations of the wall properties in Blasius and plane channel flow. For Blasius flow, the Reynolds number is varied through changes in the boundary layer thickness: different values of R correspond to different streamwise locations, the mean flow velocity being held constant. It follows that the effective non-dimensional spring stiffness increases with the Reynolds number, so at large enough values of R the wall behaves as if it were rigid. In contrast, for the case of channel flow, the fact that the Reynolds number is varied via changes in the mean flow velocity has the consequence that the effective wall parameters all decrease as R increases, with the exception of

† If the fluid is taken to be water and the channel half-width is 1 mm, then the curve for a non-dimensional spring stiffness of $K = 6 \times 10^{7}$ corresponds to a Kramer surface that has dimensional properties in the range considered by these authors; in particular it closely matches a wall with Young's modulus $E = 0.5 \times 10^{6}$ N m^{-2}.

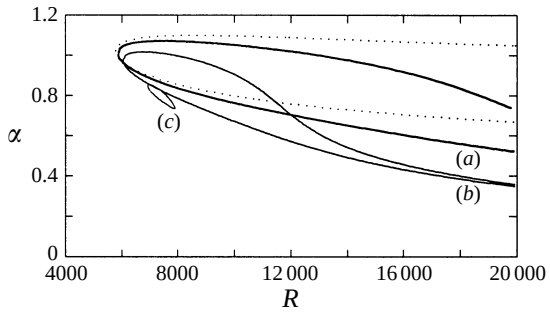

FIGURE 1. Neutral curves for the Tollmien–Schlichting instability. The dotted line is for the rigid-walled case. The solid lines correspond to compliant walls with (*a*) $K = 6\times10^7$, (*b*) $K = 2\times10^7$, (*c*) $K = 1\times10^7$, and $B = 4K$, $m = 2$, $T = d = 0$.

the wall mass which remains unchanged. Thus, the stabilizing effect of the channel walls is enhanced at large Reynolds numbers and it is not surprising that the neutral curves become confined to finite values of R. Similar results were found by Hains & Price (1962) for channels with walls modelled as tensioned membranes.

Figure 2 shows the effect of wall damping on the Tollmien–Schlichting mode. In agreement with earlier studies, it can be seen to be weakly destabilizing. Anticipating the results of the analysis of flow-induced surface instabilities given later, figure 3 displays neutral curves for travelling wave flutter. The wall parameters are the same as those taken in figure 2, except that for the damped wall the level of damping has been reduced by a factor of a hundred. For travelling wave flutter, wall damping can be seen to act in the conventional stabilizing fashion. Furthermore, the effect is far stronger than that found for the Tollmien–Schlichting waves. Even for the low level of damping considered (recall that the effective level of damping is determined by d/R), the onset of travelling wave flutter is postponed to an appreciably higher Reynolds number.

4. Flow-induced surface instabilities

We will now develop an approximate analytic theory for the description of the flow-induced surface instabilities which occur when the channel walls are made sufficiently compliant. The approach taken is similar to that which has been used in previous work for the case of Blasius flow. However, in many respects the theory is more straightforward for the channel, owing to the relative simplicity of the mean flow profile $U = 1 - y^2$. In particular, the various integrals that arise in calculating the perturbation fluid pressure at the upper channel wall are easier to evaluate. Thus, treating channel flow as a model problem, we will identify forms of behaviour that would be difficult to discern for the case of Blasius flow.

In §3 the governing equation describing the wall motion was used to provide boundary conditions to be imposed on the fluid. In this way an eigenvalue problem arises in which the wall motion equation only appears implicitly. The equation of motion for the fluid, i.e. the Orr–Sommerfeld equation, plays the primary role. For flow-induced surface instabilities the roles of the wall equations and the fluid equations can be reversed. Approximate expressions for the fluid pressure at the wall are first derived. These are then substituted into the wall motion equation to give an analytic dispersion relation from which eigenvalues can be obtained directly.

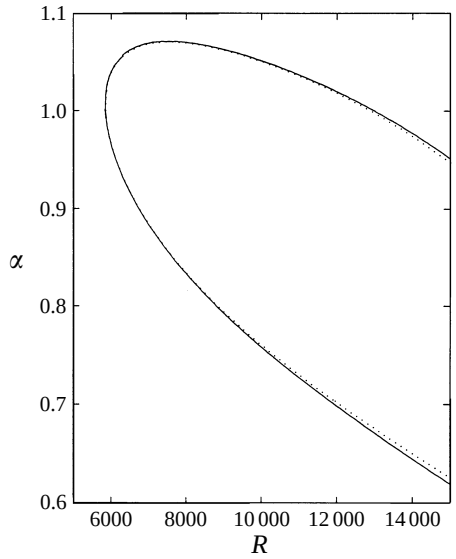

FIGURE 2. Neutral curves showing the effect of wall damping on the Tollmien–Schlichting instability. Dotted line $d = 0$, solid line $d = 1000$. The other wall parameters are $K = 6 \times 10^7$, $B = 4K$, $m = 2$, $T = 0$.

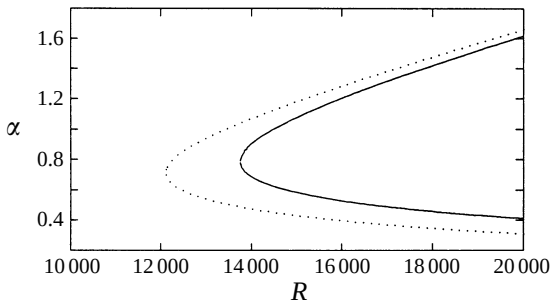

FIGURE 3. Neutral curves showing the effect of wall damping on travelling wave flutter. Dotted line $d = 0$, solid line $d = 10$. The other wall parameters are the same as in figure 2.

4.1. *Inviscid shear layer theory*

Inviscid perturbations from the mean flow $U = 1 - y^2$ are governed by Rayleigh's equation

$$(U - c)(\mathrm{D}^2 - \alpha^2)\phi - U''\phi = 0\,, \tag{18}$$

where $c = \omega/\alpha$ is the phase speed and, as before, ϕ is the profile of the disturbance streamfunction. There are two linearly independent solutions, which can be obtained via expansion in the wavenumber α:

$$\phi_1 = (U - c)\left(1 + \alpha^2 \int_{y_0}^{y} \frac{1}{(U-c)^2}\,\mathrm{d}y \int_{y_0}^{y} (U-c)^2\,\mathrm{d}y + \cdots\right), \tag{19}$$

$$\phi_2 = (U - c)\left(\int_{y_0}^{y} \frac{1}{(U-c)^2}\,\mathrm{d}y + \alpha^2 \int_{y_0}^{y} \frac{1}{(U-c)^2}\,\mathrm{d}y \int_{y_0}^{y} (U-c)^2\,\mathrm{d}y \int_{y_0}^{y} \frac{1}{(U-c)^2}\,\mathrm{d}y + \cdots\right). \tag{20}$$

These expressions were first obtained by Heisenberg (1924). The lower limit y_0 in the integrals is arbitrary. The path of integration needs to be specified when there is a critical point, i.e. when $0 < c_r < 1$, where c_r is the phase speed of a near-neutral wave. If we choose to take $y_0 = 0$, then the two solutions ϕ_1, ϕ_2 correspond to symmetric and antisymmetric disturbances respectively. Continuing to restrict attention to the symmetric case, we take

$$\phi = A\,(U-c)\left(1+\alpha^2\int_0^y \frac{1}{(U-c)^2}\,\mathrm{d}y\int_0^y (U-c)^2\,\mathrm{d}y+\cdots\right), \tag{21}$$

where A is some constant. For inviscid disturbances the single boundary condition on the fluid at the upper wall takes the form

$$\phi(1) = c\,\eta\,. \tag{22}$$

The constant A can thus be determined as

$$A = \frac{-\eta}{1+\alpha^2\displaystyle\int_0^1 \frac{1}{(U-c)^2}\,\mathrm{d}y\int_0^y (U-c)^2\,\mathrm{d}y+\cdots}\,. \tag{23}$$

Using the y-momentum equation for inviscid disturbances, the perturbation fluid pressure at the upper wall can be calculated from equation (13). Hence we obtain

$$p(1) = \alpha^2\mathscr{P}(\alpha,c)\,\eta \tag{24}$$

where

$$\mathscr{P}(\alpha,c) = \frac{\displaystyle\int_0^1 (U-c)^2\,\mathrm{d}y+\alpha^2\int_0^1 (U-c)^2\,\mathrm{d}y\int_0^y \frac{1}{(U-c)^2}\,\mathrm{d}y\int_0^y (U-c)^2\,\mathrm{d}y+\cdots}{1+\alpha^2\displaystyle\int_0^1 \frac{1}{(U-c)^2}\,\mathrm{d}y\int_0^y (U-c)^2\,\mathrm{d}y+\cdots}\,. \tag{25}$$

Substituting this expression for the wall pressure into the governing equation (4) for the wall motion then gives the dispersion relation

$$m\left(c^2-c_0^2\right)+\mathscr{P}(\alpha,c)+\mathrm{i}\left(c/\alpha\right)\bar{d}=0 \tag{26}$$

where

$$c_0 = \frac{1}{U_m}\left[\frac{1}{m}\left(\bar{B}\alpha^2+\bar{T}+\frac{\bar{K}}{\alpha^2}\right)\right]^{1/2} \tag{27}$$

is the dimensionless free wave speed for the wall at a given wavenumber α. The wall mass m is non-dimensionalized in the manner indicated earlier, but, since viscosity is no longer inherent to the problem, the other wall parameters have been treated in a different fashion. Thus we define

$$\bar{d} = \frac{d^*}{\rho U_m}\,,\ \bar{B} = \frac{B^*}{\rho h^3}\,,\ \bar{T} = \frac{T^*}{\rho h}\,,\ \bar{K} = \frac{K^* h}{\rho}\,. \tag{28}$$

The damping parameter $\bar{d}$ is non-dimensional, but all the other quantities have the dimensions of a squared velocity. This is convenient for obtaining expressions for the critical velocities that determine the onset of instability.

The expression (25) for the quantity $\mathscr{P}$ can be expanded formally as

$$\mathscr{P}(\alpha,c) = P_0(c)+\alpha^2 P_1(c)+\cdots \tag{29}$$

where the first two expansion coefficients are given by

$$P_0(c) = \int_0^1 (U-c)^2 \, \mathrm{d}y, \tag{30}$$

$$P_1(c) = -\int_0^1 \frac{1}{(U-c)^2} \, \mathrm{d}y \left(\int_0^y (U-c)^2 \, \mathrm{d}y \right)^2 . \tag{31}$$

(Some manipulation of the integrals is required in order to obtain P_1 in the form stated.) Using the parabolic profile of U, the integral for P_0 is simple to evaluate, giving

$$P_0(c) = c^2 - \tfrac{4}{3}c + \tfrac{8}{15}. \tag{32}$$

The integral defining P_1 is also straightforward to evaluate, though account needs to be taken of the singularity which occurs when there is a critical point. The detailed form of the integral is given later.

Use of the expansion (29) fails to make apparent some important features contained within the inviscid shear layer theory. In particular, it hinders the identification of a branch of inviscid solutions which corresponds to the Tollmien–Schlichting waves. Nevertheless, we will begin by employing the expansion in an uncritical manner, since it affords a means of obtaining tractable approximations to the inviscid dispersion relation. Moreover, such a form of expansion was utilized in previous studies for the case of Blasius flow (Carpenter & Garrad 1986; Carpenter & Gajjar 1990).

For small enough wavenumbers α we can hope to obtain an acceptable approximation by replacing $\mathscr{P}$ with P_0. This yields the dispersion relation

$$m\left(c^2 - c_0^2\right) + c^2 - \tfrac{4}{3}c + \tfrac{8}{15} + \mathrm{i}\left(c/\alpha\right)\bar{d} = 0 \,, \tag{33}$$

which can be solved to obtain stability boundaries. The analysis is simpler for the case of temporal instabilities, for which c is allowed to be complex-valued whilst α is kept real. (Critical layer and wall layer effects, which are discussed in detail later, are more readily treated within the framework of a temporal analysis. Restricting α to be real also avoids the necessity of isolating any evanescent modes (Carpenter & Morris 1990).) When there is no wall damping, (33) is a quadratic in c with real coefficients. Its two solutions are

$$c = \frac{1}{m+1}\left(\tfrac{2}{3} \pm r\right) \tag{34}$$

where

$$r = \left(m(m+1)c_0^2 - \tfrac{4}{45}(6m+1)\right)^{1/2} .$$

Thus there are no real-valued solutions for c if

$$c_0^2 \leqslant \frac{4}{45}\frac{6m+1}{m(m+1)} \tag{35}$$

which, using (27), shows that there is instability provided $U_m \geqslant U_f$, where

$$U_f = \frac{3}{2}\left(\frac{5(m+1)}{6m+1}\right)^{1/2} U_0 \,, \tag{36}$$

and U_0 is defined by

$$U_0 = \left(\min_{\alpha} \left[\bar{B}\alpha^2 + \bar{T} + \frac{\bar{K}}{\alpha^2} \right] \right)^{1/2} . \tag{37}$$

The subscript chosen to label the critical flow velocity U_f denotes the identification of

the instability as flutter instability. It has also been described as a Kelvin–Helmholtz instability by Benjamin (1960) and Landahl (1962), owing to its resemblance to the well-known shear-flow instability. (Throughout this paper the term 'flutter' will be reserved for the strong instability that can arise when the two branches of solutions associated with flow-induced surface waves coalesce or, more generally, interact.) The quantity U_0 is $m^{1/2}$ times the minimum of the dimensional free wave speed. In effect, it characterizes the lowest possible stiffness of the walls. There is no difficulty in showing that the minimum occurs for the non-dimensional wavenumber

$$\alpha_c = \left(\frac{\bar{K}}{\bar{B}}\right)^{1/4} \tag{38}$$

and takes the value

$$U_0 = \left(2(\bar{B}\bar{K})^{1/2} + \bar{T}\right)^{1/2} = \left(\frac{2(B^*K^*)^{1/2} + T^*}{\rho h}\right)^{1/2} . \tag{39}$$

These results are virtually identical to those given in equations (3.6) and (3.7) of Carpenter & Garrad (1986) for the Blasius boundary layer, provided the displacement thickness is used instead of the half-channel width. It also turns out that $1/\alpha_c$ – or, equivalently, the wavelength of the slowest free wave – is, arguably, the most important lengthscale characterizing the compliant wall. It is not completely clear why this is so. It was found by Carpenter (1987) and Carpenter & Morris (1990) to be a key parameter in optimizing the compliant-wall properties for maximum transition delay in the Blasius boundary layer, the walls with the best performance having values of α_c close to the wavenumber, α_{ts}, of the most unstable Tollmien–Schlichting wave. A heuristic explanation for this is attempted in Davies (1995). In the present context it will be shown in §4.5 that the character of the eigenmode spectrum is strongly dependent on whether $\alpha_c \ll \alpha_{ts}$ or they are comparable in value.

If small levels of wall damping are introduced, then the solutions (34) are perturbed to

$$c = \frac{1}{m+1}\left(\frac{2}{3} \pm r - \frac{\mathrm{i}\bar{d}}{2\alpha}\left(1 \pm \frac{2}{3r}\right)\right) . \tag{40}$$

In this case instability sets in when $r = 2/3$, which implies that $c = 0$. Thus, the instability takes the form of a standing wave at its onset. From the approximated dispersion relation (33), it can be seen that waves with $c = 0$ are only possible if there is a solution to

$$c_0^2 = \frac{8}{15m} \tag{41}$$

for some value of the wavenumber α. This yields the condition that $U_m \geqslant U_d$, where it is simple to show that

$$U_d = \left(\tfrac{15}{8}\right)^{1/2} U_0 . \tag{42}$$

The subscript d indicates that the instability can be identified as divergence. For flow velocities U_m slightly greater than U_d, the divergence instability takes the form of a slowly travelling wave, which propagates in the downstream direction. From the results (36) and (42) it can be confirmed that $U_f > U_d$, so divergence will always set in at a lower flow speed than the flutter instability whenever there is non-vanishing wall damping.

For the special case of a channel with compliant walls described as unsupported tensioned membranes, i.e. when $K^* = B^* = 0$, $T^* \neq 0$, $m^* \neq 0$, expressions equivalent

to (36), (42) were noted by Green & Ellen (1972). With such a restricted wall model, the dimensional free-wave speed takes the constant value $(T^*/m^*)^{1/2}$, independent of the wavenumber. According to the lowest-order approximation obtained from the inviscid theory, there is then no specific critical wavenumber at which instability sets in: both flutter and divergence become unstable for all disturbance wavelengths as soon as the respective onset speed has been exceeded. It would appear that Green & Ellen were unable to use their expressions for onset velocities† to provide a detailed analysis of the results they obtained by direct numerical solution of the Orr–Sommerfeld equation. This shortcoming stems from the fact that they did not go on to study the travelling wave flutter instability.

4.2. *Travelling wave flutter*

We now investigate the effect of including the critical point in the inviscid theory. For neutral disturbances with $0 < c < 1$ there is a point $y_c = (1-c)^{1/2}$ where $U(y_c) = c$. This is a singular point of Rayleigh's equation and gives rise to a logarithmic singularity in the integrals defining the solution for ϕ given in the previous section. Although such an inviscid solution will not be valid in the immediate vicinity of the critical point, it still holds elsewhere, provided the path in the integrals is suitably deformed. By matching solutions of the inviscid problem to solutions of the Orr–Sommerfeld equation in the limit of large Reynolds numbers, the appropriate path can be determined. Since $U'(y_c) < 0$, the integral path needs to be indented above the real axis at the critical point. This procedure only gives acceptable results provided there is sufficient separation between the critical layer and the viscous layer at the upper wall (Drazin & Reid 1981). (When the two layers overlap, it may still be possible to obtain good predictions, as has been demonstrated by Healey (1995) in connection with the Tollmien–Schlichting instability for Blasius flow over a rigid wall.)

In the calculation of the fluid perturbation pressure at the upper wall, taking account of the critical point in the manner just described introduces a non-zero imaginary part into the quantity $\mathscr{P}$ occurring in equation (24). This stems from the singularity at $y_c = (1-c)^{1/2}$ in the integral for the expansion coefficient P_1 defined in (31). The imaginary part of $\mathscr{P}$ gives rise to a phase difference between the wall pressure and wall displacement, which allows the fluid to do work on the wall. Thus there is the possibility of a destabilizing energy transfer to the wall. Such a mechanism was first identified for water waves by Miles (1957). The same mechanism was shown by Benjamin (1960) to apply in the case of flow over a compliant wall. More recently, Carpenter & Garrad (1986) have introduced the term travelling wave flutter to describe the associated instability.

To study the onset of travelling wave flutter instability we first solve the dispersion relation (26) in the same way as in the last section, i.e. starting from the approximation $\mathscr{P} = P_0$. If $U_m < U_f$ and there is no wall damping, this gives two neutrally stable solutions. We can then consider how these solutions are perturbed when we replace P_0 by $P_0 + \alpha^2 P_1$. The solutions are shifted from c to $c + \Delta c$, where

$$\Delta c = \frac{-\alpha^2 P_1}{2(m+1)c - \frac{4}{3}}\,. \tag{43}$$

It will be shown that if $0 < c < 1$ the imaginary part of P_1 is negative. Thus we

† In order to facilitate comparisons with the Tollmien–Schlichting instability, they gave their results in terms of critical Reynolds numbers. Since the Reynolds number is varied only through the centreline velocity of the mean flow, this is equivalent to giving critical flow velocities.

get instability provided we also have $c > 2/3(m+1)$. From the form of the solutions given in (34) it can be seen that this further condition holds for one of the waves but not for the other. Only the wave which travels the faster in the downstream direction can become unstable; the other wave is stabilized if it propagates downstream and unaffected if it propagates upstream. The onset of the instability is thus determined by the condition that there is a wave with $c = 1$. (The stability boundary at $c = 2/3(m+1)$ coincides with that which is predicted for the flutter instability. As will be seen below, it corresponds to a higher flow velocity than that needed to destabilize travelling wave flutter.) Substituting $c = 1$ into the dispersion relation (33), where $\mathscr{P}$ is replaced by P_0, gives the condition

$$c_0^2 = 1 + \frac{1}{5m} \tag{44}$$

This is only possible provided $U_m \geqslant U_t$, where

$$U_t = \left(\frac{1}{m + \frac{1}{5}}\right)^{1/2} U_0 \,. \tag{45}$$

Using the results (42) and (45), it is straightforward to show that divergence sets in at a lower flow speed if the plate mass satisfies $m < 1/3$, whilst travelling wave flutter sets in first if $m > 1/3$. It may also be checked, using (36), that the flutter instability is predicted to always set in at an even higher flow speed.

For vanishingly small values of the plate mass m, the critical velocity U_t tends to a finite limit, so the travelling wave flutter instability persists. This is in apparent contrast to the situation found in Blasius flow (Carpenter & Garrad 1986), where the corresponding formula is

$$U_t^B = \left(\frac{1}{m}\right)^{1/2} U_0 \,. \tag{46}$$

In this case the instability sets in at indefinitely high flow speeds as m decreases to zero. The difference between the two cases is connected to the assumption that potential theory provides a good first approximation for the flow over a flat plate. In previous studies of Blasius flow, the critical layer has been accounted for by perturbing the expression for the wall pressure from the result given by potential theory. If we assumed that the critical layer could be treated in the same way for channel flow, then the formula obtained for the critical velocity would be identical to the one given for Blasius flow. However, when the parabolic profile of the channel flow is considered, an effective mass is contributed by the fluid. This appears as the fraction $1/5$ in the denominator in (45).

These remarks suggest that a re-examination of the situation for Blasius flow may be in order. By analogy with the result found for channel flow, it could be anticipated that the effect of explicitly considering the profile of the mean flow would be to introduce a fluid mass to be added to the wall mass in (46). The fact that this is actually the case is implicit in the results of Carpenter & Gajjar (1990). Restricting attention to two-dimensional disturbances, and only retaining inviscid terms, their expression [3.32] for the fluid perturbation pressure at the wall can be written as

$$p_w^B = -\left(\alpha(1-c)^2 + \alpha^2\left[1 - \frac{1}{H} - 2(1-c)\right] - \alpha^2(1-c)^2 I_\infty\right)\eta \tag{47}$$

where H is the ratio of displacement to momentum thickness ($= 2.591$ for the Blasius velocity profile) and the term involving the quantity I_∞ accounts for the phase shift

due to the critical layer. The first term in (47) gives the pressure according to potential theory. The terms enclosed in the square brackets can be interpreted as the mean-flow profile correction to the result given by potential theory. Following a similar procedure to that described above we obtain

$$U_t^B = \left(\frac{1}{m+1-1/H}\right)^{1/2} U_0 \tag{48}$$

for the onset flow speed of travelling wave flutter. Thus for Blasius flow it can also be argued that travelling wave flutter will persist for vanishingly light plates. However, it should be noted that the physical interpretation of the expression giving the onset flow speed is less straightforward for Blasius flow than it is for the channel. For channel flow there is a natural lengthscale, given by the channel half-width h, which can be used to non-dimensionalize the wall mass. There is no such lengthscale available for Blasius flow. Instead, use must be made of the boundary layer displacement thickness δ^*, which is only defined locally at each streamwise position. Writing (48) in explicit dimensional form gives

$$U_t^B = \left(\frac{2(B^*K^*)^{1/2} + T^*}{m^* + (1-1/H)\,\rho\delta^*}\right)^{1/2}. \tag{49}$$

It can be seen that the fluid mass to be added to the wall mass depends on the streamwise location via the local boundary layer thickness. The effective fluid mass increases downstream.

We may well expect the inclusion of the critical layer to have some effect on the onset of the divergence instability. Divergence is associated with the solution given by (34) with the minus sign taken. Instability is predicted when the corresponding wave changes its direction of propagation from upstream to downstream. It has been noted previously that when the critical layer is accounted for, the shift Δc produced in the velocity of this wave is such that it is stabilized if it propagates downstream. Thus, we would expect the critical layer to have a stabilizing effect on divergence. However, without further detailed investigation, we cannot be sure that the onset of divergence instability will be postponed to higher flow velocities. Divergence sets in when $c = 0$, which is precisely where the theory presented for the critical layer would be expected to become invalid.

The effects on stability of including the critical layer can be described from a broader point of view using the energy analysis developed by Landahl (1962) and Benjamin (1963). Waves are classed as type A, B, or C using the concept of an activation energy†. This classification can then be employed to understand the effects of irreversible energy transfers to and from the compliant wall. Class-A waves are stabilized/destabilized when there is a transfer of energy to/from the wall. For Class-B waves the opposite is true. Class-B behaviour is what would be anticipated in more conventional circumstances. Waves described as Class C are relatively indifferent to the effects of irreversible energy transfer. They are destabilized by processes involving conservative energy exchanges. Thus the flutter instability can be viewed as Class C. Travelling wave flutter is Class B, since it is destabilized when there is a transfer of energy to the wall due to the critical layer. For divergence the same energy transfer mechanism has a stabilizing effect, so divergence appears to be a Class-A instability.

† The terms negative- and positive-energy waves have also been used to denote Class A and B waves. The alternative nomenclature stems from the independent discovery of similar physical principles in the context of plasma physics (Briggs 1964).

The utility of the energy classification can be seen when the effect of introducing wall damping is considered within the same framework. Wall damping provides a means of irreversibly removing energy from the wall. Thus the fact that divergence is destabilized by wall damping is seen to be consistent with its Class-A behaviour with respect to the critical layer. Similarly, we would expect the travelling wave flutter instability to display its Class-B character by being stabilized by damping. This can be confirmed directly by inspecting (40). The solution given by taking the plus sign corresponds to travelling wave flutter.

We now return to the evaluation of the quantity $P_1(c)$, the imaginary part of which is associated with the effect of the critical layer on stability. Using the parabolic form of the velocity profile U, the integral in (31) can be manipulated to give

$$P_1(c) = -\frac{1}{225}\left(Q(c) + 32(1-c)^4 \int_0^1 \frac{1}{(1-c)-y^2}\,\mathrm{d}y\right) \tag{50}$$

where

$$Q(c) = \tfrac{9}{7} - \tfrac{42}{5}(1-c) + \tfrac{97}{3}(1-c)^2 - 64(1-c)^3 - \frac{32}{c}(1-c)^4\,.$$

The $1/c$ singularity in $Q(c)$ suggests the breakdown of the present approximation for small values of c. When the phase velocity is such that $0 < c < 1$, the path in the remaining integral term in (50) needs to be indented above the critical point at $y_c = (1-c)^{1/2}$. A simple calculation then gives the imaginary part of P_1 as

$$\mathrm{Im}\,(P_1(c)) = -\frac{16\pi}{225}(1-c)^{7/2}\,. \tag{51}$$

So $\mathrm{Im}\,(P_1) < 0$, as claimed earlier. If there is no critical layer, then for real values of c the integral appearing in (50) is real and so is P_1.

From the expressions (32) and (50) we can specify both P_0 and P_1 in terms of known functions of the wave velocity c. Using the approximation $\mathscr{P} = P_0 + \alpha^2 P_1$ in the dispersion relation (26), we obtain an equation written explicitly in terms of c and α. It is then a straightforward matter to solve this equation numerically in order to determine the values of the wave velocity associated with each value of the wavenumber. The computational requirements are very slight, compared with what is needed for the direct numerical solution of the Orr–Sommerfeld equation.

4.3. *Viscous wall layer corrections*

Results obtained by solving (26) in the manner outlined above can be shown to provide a fairly accurate basis for describing the travelling wave flutter instability. Nevertheless, it is still informative to see if the theory can be further improved by taking account of the effects of the viscous wall layer in the fluid. For channel flow this can be achieved with little additional labour. In contrast, improving the corresponding theory for Blasius flow is quite difficult (Carpenter & Gajjar 1990), partly because of the need to account carefully for the details of the mean flow profile.

For large values of the Reynolds number R there are two regions where viscous effects can be considered important. In addition to the critical layer centred on the position of the critical point, there is a viscous layer adjacent to the wall. These layers have widths of $O\{(\alpha R)^{-1/3}\}$ and $O\{(\alpha R)^{-1/2}\}$ respectively. It is assumed that they do not overlap. Violation of this assumption can be expected to cause the breakdown of the theory for small enough values of c. We also suppose that there are approximate

solutions to the Orr–Sommerfeld equation which take the form

$$\phi = A\,\Phi + a\,\phi_v \tag{52}$$

where Φ is an inviscid solution determined as before, and ϕ_v is a rapidly varying viscous solution which is insignificant outside the wall layer. The constants A and a are determined by the boundary conditions on the fluid at the wall. The composite solution (52) is invalid within the critical layer, since no direct account of viscosity is taken there. However, it will be shown that this is not important so far as the calculation of the wall pressure is concerned.

The inviscid part of the solution is specified in the same form as the solution considered previously. We take it to be defined by

$$\Phi = (U-c)\left(1+\alpha^2\int_0^y \frac{1}{(U-c)^2}\,\mathrm{d}y\int_0^y (U-c)^2\,\mathrm{d}y + \cdots\right). \tag{53}$$

The viscous solution is obtained by examining the Orr–Sommerfeld equation in the vicinity of the wall. Introducing the scaled normal distance from the wall $\hat{y} = (1-y)/\epsilon$, where $\epsilon = (\alpha R)^{-1/2}$, the Orr–Sommerfeld equation can be written as

$$(\hat{\mathrm{D}}^4 + \mathrm{i}c\hat{\mathrm{D}}^2)\hat{\phi} = O(\epsilon) \tag{54}$$

with $\hat{\mathrm{D}} = \mathrm{d}/\mathrm{d}\hat{y}$ and $\hat{\phi}(\hat{y}) = \phi(y)$. This has the general solution

$$\hat{\phi}(\hat{y}) = C_1 + C_2\hat{y} + C_3\exp(\mathrm{e}^{-\mathrm{i}\pi/4}c^{1/2}\,\hat{y}) + C_4\exp(-\mathrm{e}^{-\mathrm{i}\pi/4}c^{1/2}\,\hat{y}) + O(\epsilon)\,. \tag{55}$$

The first two terms correspond to the inviscid solution, whilst the third grows rapidly beyond the wall layer. The fourth term decays away from the wall and can thus be identified with the desired viscous solution ϕ_v. Hence we define

$$\phi_v(y) = \exp\left(-\mathrm{e}^{-\mathrm{i}\pi/4}(\alpha c R)^{1/2}\,(1-y)\right). \tag{56}$$

This is normalized so that $\phi_v(1) = 1$.

Using the boundary conditions (7) at the wall, the constants A, a can be obtained in the general form

$$A = \left(\frac{c\phi'_{v1} + U'_1\phi_{v1}}{\Phi_1\phi'_{v1} - \phi_{v1}\Phi'_1}\right)\eta, \quad a = -\left(\frac{c\Phi'_1 + U'_1\Phi_1}{\Phi_1\phi'_{v1} - \phi_{v1}\Phi'_1}\right)\eta \tag{57}$$

where we have introduced the notation $\Phi_1 = \Phi(1)$, $\Phi'_1 = \mathrm{D}\Phi(1)$ etc. Making use of the facts that $\phi_{v1} = 1$ and ϕ'_{v1} is $O(1/\epsilon)$, these expressions can expanded in terms of ϵ to give

$$A = \left(1 + \frac{1}{\phi'_{v1}}\left(\frac{U'_1}{c} + \frac{\Phi'_1}{\Phi_1}\right)\right)\frac{c\eta}{\Phi_1} + O(\epsilon^2), \tag{58}$$

$$a = -\frac{1}{\phi'_{v1}}\left(\frac{U'_1}{c} + \frac{\Phi'_1}{\Phi_1}\right)c\eta + O(\epsilon^2)\,. \tag{59}$$

The constant a is $O(\epsilon)$. Thus it can be seen that retaining an $O(\epsilon)$ term in the definition of ϕ_v would have made no difference to the $O(\epsilon^2)$ approximation for the composite solution ϕ.

The quantity in brackets which appears multiplied by $1/\phi'_{v1}$ in the expressions for both the constants can be rewritten in terms of the previously defined quantity $\mathscr{P}(\alpha, c)$. It is straightforward to see that the definition of $\mathscr{P}$ given in §4.1 amounts to taking

$$\mathscr{P} = -\frac{c}{\Phi_1}\int_0^1 (U-c)\,\Phi\,\mathrm{d}y\,. \tag{60}$$

If the inviscid wall pressure associated with the profile Φ is computed using the x-momentum equation for inviscid disturbances, and then again using the y-momentum equation, the following equality can be derived:

$$U_1'\Phi_1 + c\Phi_1' = -\alpha^2 \int_0^1 (U-c)\Phi \, \mathrm{d}y, \tag{61}$$

from which it follows that

$$\frac{U_1'}{c} + \frac{\Phi_1'}{\Phi_1} = \frac{\alpha^2}{c^2}\mathscr{P}. \tag{62}$$

Hence we can finally write

$$A = \left(1 + \frac{\mathrm{e}^{\mathrm{i}\pi/4}}{(\alpha c R)^{1/2}}\frac{\alpha^2}{c^2}\mathscr{P}\right)\frac{c\eta}{\Phi_1} + O(\epsilon^2), \tag{63}$$

$$a = -\left(\frac{\mathrm{e}^{\mathrm{i}\pi/4}}{(\alpha c R)^{1/2}}\frac{\alpha^2}{c^2}\mathscr{P}\right) c\eta + O(\epsilon^2) \tag{64}$$

and thus obtain

$$\phi = \left(\frac{\Phi}{\Phi_1} + \frac{\mathrm{e}^{\mathrm{i}\pi/4}}{(\alpha c R)^{1/2}}\frac{\alpha^2}{c^2}\mathscr{P}\left(\frac{\Phi}{\Phi_1} - \phi_v\right)\right) c\eta \tag{65}$$

as the composite solution to the Orr–Sommerfeld equation. This is an $O(\epsilon^2)$ approximation to the exact solution, except within the critical layer.

The wall pressure corresponding to an exact solution of the Orr–Sommerfeld solution can be found using the expression (12). We aim to derive an $o(\epsilon)$ approximation for the wall pressure by substituting the composite solution (65) for ϕ. At this level of accuracy the terms in (12) which involve the factor $1/R$ can be shown to be negligible. The wall derivative satisfies $\mathrm{D}\phi(1) = -U'(1)\eta$, and consequently has a magnitude of $O(1)$. Thus the term involving this derivative gives an $O(\epsilon^2)$ contribution to the pressure. (Note that this term is in fact just an $O(1)$ multiple of the normal viscous stress acting at the wall. We ought to be able to neglect it in order to maintain consistency with the previous assumption that the forcing of the wall is given by the fluid pressure alone.) The integral multiplied by $1/R$ would be expected to have a similar magnitude to the integral appearing in the first term. Thus by comparison it can be omitted as giving rise to only an $O(\epsilon^2)$ quantity.

Having neglected the terms in (12) containing factors of $1/R$, we are left with a single integral which determines the wall pressure. Since the constant a is $O(\epsilon)$ and the viscous solution ϕ_v is negligible outside the wall layer, which itself has width $O(\epsilon)$, it can be seen that the contribution of the viscous part of the composite solution to the integral is $O(\epsilon^2)$. Hence the integral, and consequently the wall pressure, can be determined using the inviscid part of the solution alone. At this point it could be objected that no account has been taken of the fact that the composite solution does not hold in the critical layer. This might invalidate the approximation procedure just described. However, it can be argued that even if an $O(1)$ viscous correction needed to be made to the solution within the critical layer, it would not affect the calculation of the wall pressure to the order of accuracy considered. The quantity $(U-c)$ vanishes at a point y_c in the critical layer, so near this point we have $(U-c) \simeq U_c'(y-y_c)$. Because $(y-y_c)$ is $O(\epsilon^{2/3})$ in the critical layer, the same must be true of $(U-c)$. Integrating an $O(1)$ multiple of $(U-c)$ across the critical layer thus gives a correction to the wall pressure which is only $O(\epsilon^{4/3})$.

Putting together the arguments given above, we arrive at the following approximation for the wall pressure:

$$p(1) = -\alpha^2 A \int_0^1 (U - c)\, \Phi \, \mathrm{d}y + o(\epsilon)\,. \tag{66}$$

On using the expression (63) for A, and applying the definition of $\mathscr{P}$ in the form given in (60), this yields

$$p(1) = \alpha^2 \left(1 + \frac{\mathrm{e}^{\mathrm{i}\pi/4}}{(\alpha c R)^{1/2}} \frac{\alpha^2}{c^2} \mathscr{P}\right) \mathscr{P}\eta + o(\epsilon). \tag{67}$$

This should be compared with the corresponding expression (24) obtained from inviscid theory. It can then be seen that the effect of accounting for the viscous wall layer is to replace $\mathscr{P}$ by $\mathscr{P}_v$ where

$$\mathscr{P}_v = \left(1 + \frac{\mathrm{e}^{\mathrm{i}\pi/4}}{(\alpha c R)^{1/2}} \frac{\alpha^2}{c^2} \mathscr{P}\right) \mathscr{P}\,. \tag{68}$$

The modification required in the inviscid dispersion relation (26) is obtained in the same way.

The stability effects of bringing the viscous wall layer into consideration can now be found in a manner analogous to that used previously in studying the critical layer. We begin by solving the dispersion relation using the first approximation $\mathscr{P}_v = P_0$. Then taking the $O(\alpha^2)$ approximation

$$\mathscr{P}_v = P_0 + \alpha^2 \left(P_1 + \frac{\mathrm{e}^{\mathrm{i}\pi/4}}{c^2 (\alpha c R)^{1/2}} P_0^2\right) \tag{69}$$

the shift in the wave velocities can be found in the same way as before. The expression for Δc corresponding to the inviscid result (43) is readily seen to be

$$\Delta c = \frac{-\alpha^2}{2\left((m+1)c - \frac{2}{3}\right)} \left(P_1 + \frac{\mathrm{e}^{\mathrm{i}\pi/4}}{c^2 (\alpha c R)^{1/2}} P_0^2\right). \tag{70}$$

In the inviscid theory, it was shown that the destabilization of travelling wave flutter is associated with the introduction of a negative imaginary part in P_1 when there is a critical layer. In physical terms, a phase difference is set up between the wall pressure and wall displacement, allowing an irreversible transfer of energy by the fluid to the wall. When the viscous wall layer is accounted for, there is a further shift in phase between the pressure and displacement. Using the result (51) for $\mathrm{Im}(P_1)$ we obtain

$$\mathrm{Im}(\Delta c) = \frac{-\alpha^2}{2\left((m+1)c - \frac{2}{3}\right)} \left(-\frac{16\pi}{225}(1-c)^{7/2} + \frac{1}{c^2 (2\alpha c R)^{1/2}} P_0^2\right). \tag{71}$$

(If there is no critical layer then the first term in the large brackets should be dropped.) From this it can be seen that, as found previously by Carpenter & Gajjar (1990) for the Blasius boundary layer, the effect of the wall layer is to stabilize travelling wave flutter, in direct opposition to the effect of the critical layer. On the basis of the energy classification discussed earlier, it would then be expected that the effect of the wall layer on divergence would be destabilizing. Formally, this can be deduced directly from (71); the solution corresponding to divergence has $c < 2/3(m+1)$. However, it should be recalled that the viscous wall layer correction was obtained under the assumption that the wall and critical layers remain well separated. Such

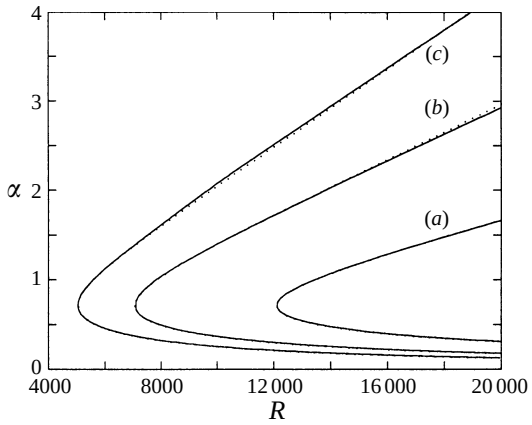

FIGURE 4. Comparison of neutral stability curves for travelling wave flutter computed via direct numerical solution of the Orr–Sommerfeld equation (solid lines) with results obtained from the analytic theory (dotted lines). The wall parameters are (*a*) $K = 6 \times 10^7$, (*b*) $K = 2 \times 10^7$, (*c*) $K = 1 \times 10^7$, and $B = 4K$, $m = 2$, $T = d = 0$.

an assumption will not be valid for the small phase speeds that, according to the lowest-order inviscid theory, mark the onset of divergence instability.

4.4. *Numerical results for travelling wave flutter*

The predictions of the approximate analytic theory for the travelling wave flutter instability are now compared with results obtained by direct numerical solution of the Orr–Sommerfeld equation. The dispersion relation obtained when the viscous wall layer is included can be solved using a slight modification of the method outlined at the end of §4.2. We just need to replace $\mathscr{P}$ by $\mathscr{P}_v$.

Figure 4 shows computed neutral stability curves for travelling wave flutter. The sets of compliant wall parameters are the same as those chosen for the Tollmien–Schlichting neutral stability curves previously plotted in §3.3. It can be seen that the agreement between results obtained from the analytic theory and the numerical solution of the Orr–Sommerfeld equation is extremely good. The curves lie directly on top of each other, except at some larger values of the wavenumber α where there is a slight discrepancy. (The analytic theory might not be expected to hold for such values of α since it relies on a low-wavenumber expansion. An explanation of why the expansion continues to give acceptable approximations even when $\alpha \approx 4$ will be given below in §4.5.2.) A comparison of the curves shown for the travelling wave flutter in figure 4 with the corresponding results for Tollmien–Schlichting waves displayed in figure 1 makes clear the opposite effects of wall compliance on the two instabilities.

The analytic theory used to obtain the curves in figure 4 contains the viscous wall layer correction described in the previous section. When the effect of viscosity is thus included, the results derived from the inviscid theory, in particular the expressions for instability onset velocities, need to be presented in terms of Reynolds numbers. This causes no difficulty, since the Reynolds number is only varied through changes in the centreline velocity of the mean flow. If we fix the dimensional channel half-width h and kinematic viscosity ν, then we can define

$$R_c = U_c h/\nu \tag{72}$$

to be the critical Reynolds number corresponding to the critical velocity U_c. To

obtain a consistent description, we also need to non-dimensionalize the compliant wall properties in the fashion described earlier in §3. This amounts to writing

$$mc_0^2 = (B\alpha^2 + T + K/\alpha^2)/R^2\ ,\ \bar{d} = d/R \tag{73}$$

for the free-wave speed and damping terms that occur in the inviscid dispersion relation (26) and the wall-layer-corrected version.

Figure 5 compares neutral stability curves computed from the approximate analytic theory with and without any wall-layer correction. It can be seen that there is a significant discrepancy between the two curves. Although the critical wavenumber is unchanged, the Reynolds number for the onset of instability is poorly predicted when the wall layer is not included. This stems from the fact that the growth rates determined from the inviscid theory with no wall-layer correction are quite weak near the expected onset. Thus the instability can be readily held in check by the stabilizing effect of the wall layer. It is straightforward to estimate the extent to which the onset of travelling wave flutter is delayed, using the result (71) which gives the net change in the temporal growth rate due to the effects of the critical and wall layers. When the wall layer is included, the phase velocity of the wave which first becomes unstable is no longer given by $c = 1$, but is instead displaced to a lower value by an amount

$$\Delta c_t = -\left(\frac{9}{16\pi}\right)^{2/7} \frac{1}{(2\alpha_c R_t)^{1/7}}\ . \tag{74}$$

The corresponding shift in the Reynolds number can then be estimated from the inviscid dispersion relation. Denoting by ΔR_t the increase in the critical Reynolds number for the onset of travelling wave flutter from the value R_t obtained when the effect of the wall layer is neglected, it is simple to show that

$$\frac{\Delta R_t}{R_t} = -\left(\frac{m+\frac{1}{3}}{m+\frac{1}{5}}\right)\Delta c_t = \left(\frac{m+\frac{1}{3}}{m+\frac{1}{5}}\right)\left(\frac{9}{16\pi}\right)^{2/7} \frac{1}{(2\alpha_c R_t)^{1/7}}\ . \tag{75}$$

Thus $\Delta R_t/R_t$ is $O(1/R^{1/7})$, and so is appreciable even for the relatively large values of R that are of current interest. For the sets of compliant wall properties used in obtaining figure 4, the fractional increases in the critical Reynolds number estimated from (75) lie in the range 15–20%. These estimates give good first approximations to the accurate values determined from either the exact solution of the wall-layer-corrected inviscid dispersion relation or the direct numerical solution of the Orr–Sommerfeld equation. For waves corresponding to points within the unstable regions shown in figure 4, results from the inviscid theory with and without the wall layer correction are in closer agreement with each other; the relative effect of the wall layer is diminished for larger growth rates.

As mentioned in the Introduction, Carpenter *et al.* (1983), Carpenter & Garrad (1985) and others, found that the inclusion of damping in the form of a viscous fluid substrate or viscoelastic losses could lead to the coalescence of the Tollmien–Schlichting and travelling-wave-flutter modes. Figure 6 shows that a similar effect can be found in the present case for sufficiently large values of the wall damping parameter d. It can be seen that the extensive region of instability associated with travelling wave flutter in the absence of wall damping is pushed back to higher Reynolds numbers when damping is introduced, whilst the region of Tollmien–Schlichting instability is enlarged. When there is no wall damping the two regions of instability overlap each other but appear to be distinct. The inclusion of sufficiently high levels of damping leads to their coalescence. The value of the wavenumber at which the neutral curves

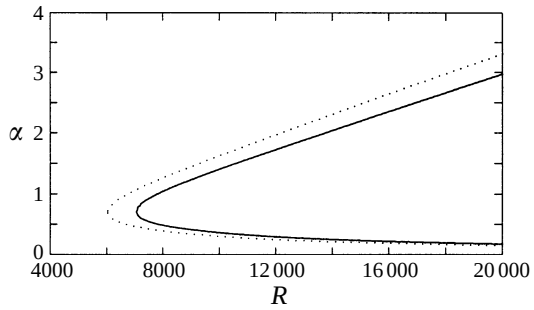

FIGURE 5. Neutral stability curves showing the effect of including (solid line) and excluding (dotted line) the wall layer in the analytic theory. The wall parameters are $K = 2 \times 10^7$, $B = 4K$, $m = 2$, $T = d = 0$.

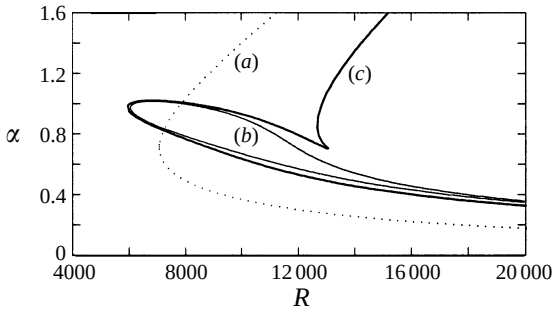

FIGURE 6. Neutral stability curves showing the merger of the Tollmien–Schlichting (TS) mode and travelling wave flutter (TWF). (*a*) TWF: $d = 0$, (*b*) TS: $d = 0$, (*c*) TS/TWF: $d = 1000$. The other wall parameters are $K = 2 \times 10^7$, $B = 4K$, $m = 2$, $T = 0$. (The curves were determined by direct numerical solution of the Orr–Sommerfeld equation.)

for travelling wave flutter and Tollmien–Schlichting instability merge is given very closely by the expression (38) for the critical wavenumber α_c derived in the inviscid theory. Furthermore, the corresponding value of R is comparable to the flutter onset Reynolds number R_f that is also predicted by the lowest-order inviscid theory. Thus it can be conjectured that the merger of Tollmien–Schlichting instability with travelling wave flutter has replaced any interaction between divergence and travelling wave flutter.

The strong effects of wall damping on the character of channel-flow stability also emerged in the recent study of Gajjar & Sibanda (1996). For a number of special cases they found that a threshold value of damping exists above which another linear neutral eigenmode is found in addition to the Tollmien–Schlichting wave. At a still higher level of damping the two neutral eigenvalues merge and no neutral Tollmien–Schlichting modes can exist when the damping exceeds this level. In other cases yet another neutral mode occurs close to the merger point but remains distinct. These sorts of results are probably related to the phenomenon of modal coalescence under discussion. It should be recalled, though, that the asymptotic structure on which Gajjar & Sibanda based their theory is really only appropriate to the Tollmien–Schlichting mode.

The same kind of qualitative behaviour in the presence of wall damping as seen in our results was noted by Green & Ellen (1972) in their numerical studies for the case of compliant channels with walls modelled as tensioned membranes. Although these

authors discussed the existence of the flow-induced surface instabilities described here as divergence and flutter, they do not appear to have been aware of the additional instability mechanism that could lead to travelling wave flutter. Thus Green & Ellen were unable to analyse some key aspects of their numerical results. We now examine the relevant part of their work in the light of the theory developed for flow-induced surface instabilities.

For walls modelled as tensioned membranes, the free wave speed is independent of the wavenumber. The lowest-order inviscid theory then predicts that the stability boundaries in the (α, R)-plane for the various flow-induced instabilities are just lines of constant R. Waves at all wavenumbers simultaneously become unstable as the flow velocity is increased beyond a critical value. The inclusion of non-vanishing wall damping displaces these boundaries in a manner that is shown in figure 7. The curve labelled (*a*) was obtained by using the approximation $\mathscr{P} = P_0 + \mathrm{i}\alpha^2 \,\mathrm{Im}(P_1)$ in the inviscid dispersion relation, i.e. by taking the lowest-order approximation for the wall pressure and then perturbing it by including the phase shift due the critical layer. The dispersion relation was then solved for points of neutral stability by matching the imaginary part of the wave velocity contributed by the critical layer to the part due to the wall damping. The selected wall parameters are the same as those used by Green & Ellen in their figure 2(i) (the wall parameter that these authors denote by c_w is just the free wave speed $(T/m)^{1/2}$). The upper branch of the neutral stability curve (*a*) is associated with travelling wave flutter, whilst the lower branch corresponds to divergence. The lower branch meets the R-axis at the divergence onset Reynolds number R_d, whilst the upper branch – were it to remain valid for large values of the wavenumber α – would asymptote to the critical Reynolds number R_t for travelling wave flutter. Both branches join at the Reynolds number R_f that should mark the onset of flutter. Curve (*b*) in figure 7 indicates the stability boundaries computed using the approximation $\mathscr{P} = P_0 + \alpha^2 P_1$, together with a viscous wall layer correction. It can be seen that the point where the two branches of the neutral curve join has moved to a lower Reynolds number than R_f. Moreover, the branch of the neutral curve identified previously as bounding the region of divergence instability now lies at higher values of α and no longer intersects the R-axis. Curve (*c*) shows the neutral stability curve computed from the direct numerical solution of the Orr–Sommerfeld equation. It is clear that the corrected inviscid theory is quite effective in locating the merger of the neutral curves for travelling wave flutter and the Tollmien–Schlichting instability. The lower branch of the stability boundary plotted by curve (*b*) appears to give an approximation to the upper branch of the Tollmien–Schlichting neutral curve, rather than delimiting the region where divergence occurs. That this may happen is perhaps not too surprising. For the upper branch of the Tollmien–Schlichting neutral curve, composite solutions of the form used in §4.3 can give valid, if somewhat coarse, approximations for Tollmien–Schlichting waves (Healey 1995).

In the next section it will be seen that the replacement of divergence by the Tollmien–Schlichting instability in determining stability boundaries is not an exceptional occurrence. The merger of the Tollmien–Schlichting and travelling-wave-flutter modes of instability also appears to be quite general. Results will be presented which show that strong interaction between the two modes can occur even in the absence of any wall damping. Before addressing such matters in more detail, we first note that there is in fact an instability region in figure 7 which can be associated with divergence. This appears for low values of the wavenumber α. (In the corresponding diagram presented by Green & Ellen, there is no such region, presumably because the computations conducted by these authors were not continued down to sufficiently

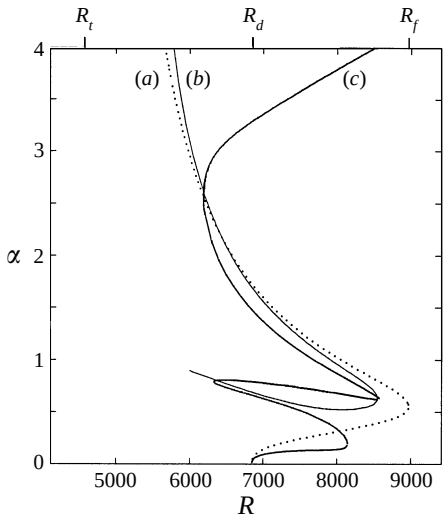

FIGURE 7. Neutral stability curves as obtained (*a*) from the inviscid theory with the approximation $\mathscr{P} = P_0 + \mathrm{i}\alpha^2\,\mathrm{Im}(P_1)$, (*b*) using the approximation $\mathscr{P} = P_0 + \alpha^2 P_1$ together with a viscous-wall-layer correction (the lower part of the curve has only been plotted for $R > 6000$), (*c*) from the full numerical solution of the Orr–Sommerfeld equation. The wall parameters are $T = 2.5 \times 10^7$, $m = 1$, $B = K = 0$, $d = 250$. The values of R labelled R_d, R_f and R_t indicate, respectively, the critical values for the onset of divergence, flutter and travelling wave flutter calculated using formulae obtained from the lowest-order inviscid approximation.

small wavenumbers.) The point of onset for the instability can be predicted exactly by employing the approximation $\mathscr{P} = P_0$ and then taking account of the phase shift across the critical layer. Near to the onset, the group velocity vanishes, which suggests that there could be an absolute instability. At larger values of the Reynolds number, the instability seems to merge with the Tollmien–Schlichting mode of instability. The neutral curves are joined at a value of R somewhat lower than that at which the travelling wave flutter and Tollmien–Schlichting modes coalesce.

4.5. *Modal coalescence and the onset of divergence instability*

Coalescence between the travelling-wave-flutter and Tollmien–Schlichting modes of instability is consistent with the energy classification developed by Landahl (1962) and Benjamin (1963). Tollmien–Schlichting waves can be categorized as being of Class A, whilst travelling wave flutter is of Class B, so in terms of irreversible energy transfer the two instabilities are complementary. This suggests that there is the theoretical possibility that the two modes could merge to form a Class C instability. Reapplying the same form of energy classification, it is not easy to comprehend the merger of the neutral curves for the divergence and Tollmien–Schlichting modes of instability, which was also reported in the previous section. Both divergence and the Tollmien–Schlichting mode are usually expected to be of Class A. Carpenter & Garrad (1986) and Lucey & Carpenter (1992) have argued that divergence is an absolute instability and more appropriately regarded as Class C. With either interpretation the apparent coalescence of the Tollmien–Schlichting and divergence modes is somewhat puzzling. In the present study, we will not pursue this matter any further. There are some other interesting features of the divergence branch of solutions which, arguably, require prior attention. In particular, for cases where the wall parameters are chosen so as to model Kramer-type compliant surfaces (for such surfaces the bending stiffness

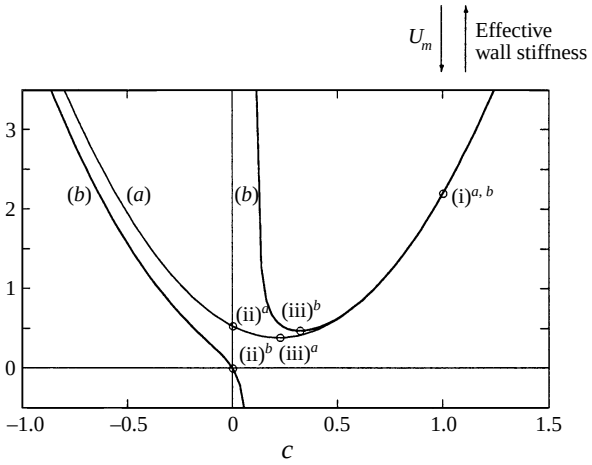

FIGURE 8. Variation with phase speed of the inertial quantities (*a*) $mc^2 + P_0(c)$, (*b*) $mc^2 + P_d^r(\alpha, c)$. The compliant wall mass is taken to be $m = 2$. In (*b*) the wavenumber is specified by $\alpha^2 = 1/2$. Permitted values of the phase velocity c can be determined from intersections between each curve and a horizontal line drawn at a height that represents the effective wall stiffness, i.e. the quantity appearing on the left-hand side of equation (83). The circles indicate the onset of instability: (i) travelling wave flutter, (ii) divergence, (iii) modal coalescence.

and spring stiffness are non-vanishing, in contrast to a tensioned membrane), it can prove difficult to obtain neutrally stable solutions of the Orr–Sommerfeld equation corresponding to divergence. In order to explain this difficulty in identifying the onset of divergence instability, we will undertake a re-examination of the inviscid shear layer theory.

4.5.1. *Singular behaviour in the inviscid shear layer theory*

Thus far, the highest-order approximation applied in the inviscid dispersion relation has been obtained by setting $\mathscr{P} = P_0 + \alpha^2 P_1$. A correction representing the effect of the viscous wall layer could also be incorporated. Both P_1 and the term associated with the viscous wall layer can be shown to have singularities at $c = 0$. (The same form of singular behaviour was documented by Carpenter & Gajjar 1990, for the case of Blasius flow.) This is rather unfortunate, since according to the lowest-order inviscid approximation, divergence should be destabilized at precisely the limit where there is a wave with zero phase velocity. Consequently, it was not too surprising to find, on making comparisons with eigenvalues obtained by solving the Orr–Sommerfeld equation directly, that the approximated dispersion relation did not always deliver reliable predictions for the branch of upstream-travelling wave solutions that was expected to give rise to the divergence instability. However, it turned out that marked disagreement could occur even when the phase speeds concerned were well removed from any supposed singularity at $c = 0$.

If we return to the definition given by equation (24), then it may be seen that, essentially, the quantity $\mathscr{P}$ is the ratio of the perturbation fluid pressure at the wall to the wall displacement. The adjustment which was made to account for the effect of the viscous wall layer led to the replacement of $\mathscr{P}$ by the quantity denoted as $\mathscr{P}_v$. This latter quantity is still defined by the ratio between the wall pressure and the wall displacement. When approximations for $\mathscr{P}$ and $\mathscr{P}_v$ were developed, no consideration was taken of the possibility that we might have a vanishing wall displacement. It

is clear that such a possibility can be realized in the case of exact solutions to the Orr–Sommerfeld equation. Both the wall displacement and the wall velocity can vanish for the Tollmien–Schlichting mode. Thus, we might expect to find singularities in $\mathscr{P}_v$ at values of α and c which correspond to Tollmien–Schlichting waves in a *rigid*-walled channel. Singularities could also occur in the inviscid quantity $\mathscr{P}$ if there were solutions of Rayleigh's equation that met the no-penetration condition for rigid walls. Such inviscid solutions would only exist, if at all, for real values of the phase speed c. When c is taken to be complex, with a non-vanishing imaginary part c_i, Rayleigh's inflection-point theorem (Drazin & Reid 1981) can be applied to rule out any possibility of a singularity. Nevertheless, the behaviour of the quantity $\mathscr{P}$ might still be expected to retain some vestige of the singularities that would be found if viscosity was fully accounted for. We can address this issue more directly by considering the original expression for $\mathscr{P}$ given in §4.1. The expression took the form of a ratio (compare equation (25))

$$\mathscr{P}(\alpha, c) = \frac{I_0(c) + \alpha^2 I_2(c) + \alpha^4 I_4(c) + \cdots}{1 + \alpha^2 I_1(c) + \alpha^4 I_3(c) + \cdots} \tag{76}$$

where

$$I_0(c) = \int_0^1 (U-c)^2 \, \mathrm{d}y,$$
$$I_1(c) = \int_0^1 \frac{1}{(U-c)^2} \, \mathrm{d}y \int_0^y (U-c)^2 \, \mathrm{d}y,$$
$$I_2(c) = \int_0^1 (U-c)^2 \, \mathrm{d}y \int_0^y \frac{1}{(U-c)^2} \, \mathrm{d}y \int_0^y (U-c)^2 \, \mathrm{d}y,$$

and the terms $I_{2k-1}(c)$, $I_{2k}(c)$ for $k > 1$ can be found from similar integrals in a recursive manner. Previously, $\mathscr{P}$ was approximated by truncating a power series expansion in α^2:

$$\begin{aligned} \mathscr{P}(\alpha, c) &= I_0(c) + \alpha^2 \left[I_2(c) - I_0(c) I_1(c) \right] + \cdots \\ &= P_0(c) + \alpha^2 P_1(c) + \cdots . \end{aligned} \tag{77}$$

It is conceivable that the use of an expansion which disguises the fact that $\mathscr{P}$ is defined by a ratio might lead to poor approximations, even if $\mathscr{P}$ itself fails to display any obvious singular behaviour. Bearing this possibility in mind, we will now examine the form taken by the quantity I_1.

After substituting the parabolic profile mean-flow $U = 1 - y^2$, the integrals that define I_1 can be manipulated to yield

$$I_1(c) = \frac{1}{15} \left(\frac{3}{2} - \frac{4}{c}(1-c) + 4(1-c) \int_0^1 \frac{y}{(1-c) - y^2} \, \mathrm{d}y \right). \tag{78}$$

When there is a critical point, the path taken when evaluating the remaining integral in (78) needs to be indented above $y_c = (1-c)^{1/2}$. A simple calculation then gives the imaginary part of I_1 as

$$\mathrm{Im}\,(I_1(c)) = \frac{2\pi}{15}(1-c)\,. \tag{79}$$

It can be seen that I_1 has a $1/c$ singularity, just as was noted previously for the quantity P_1.

4.5.2. *Approximation of the inviscid dispersion relation*

The singular behaviour found when c is small can be avoided if the truncated expansion $\mathscr{P} = P_0 + \alpha^2 P_1$ is replaced by the rational approximation

$$P_d(\alpha, c) = \frac{I_0(c) + \alpha^2 I_2(c)}{1 + \alpha^2 I_1(c)} = P_0(c) + \frac{\alpha^2 P_1(c)}{1 + \alpha^2 I_1(c)} \,. \tag{80}$$

This does not have any singularity at $c = 0$. In fact, it is easy to check that

$$\lim_{c \to 0} P_d(\alpha, c) = 0 \tag{81}$$

when α is non-zero (the behaviour for $\alpha = 0$ will be discussed later). (Reference should be made to the explicit expression (50) for the function P_1 that was given at the end of §4.2.) Similarly, it can be shown that

$$P_d(\alpha, 1) = \frac{1}{5}\left(\frac{1 + \frac{1}{14}\alpha^2}{1 + \frac{1}{10}\alpha^2}\right), \tag{82}$$

which explains why, even for α^2 of $O(1)$, an expansion of the form (77) was found to give acceptable results for the onset of travelling wave flutter instability. (It is interesting to note that the function $\mathscr{P}(\alpha, 1)$ can be determined exactly, using a closed-form solution of Rayleigh's equation. Details are given in Appendix A.)

The consequences of using different approximations for $\mathscr{P}$ are easier to illustrate if we first rewrite the dispersion relation (26) as

$$\frac{1}{U_m^2}\left(\bar{B}\alpha^2 + \bar{T} + \frac{\bar{K}}{\alpha^2}\right) = mc^2 + \mathscr{P}(\alpha, c) \,. \tag{83}$$

This can be interpreted as defining a balance between an effective wall stiffness and the combined inertia of the wall and fluid. (For simplicity, we have set the wall damping term to zero.) In figure 8 curve (*a*) plots the variation, with the phase speed, of the quantity that defines the combined inertia when the approximation $\mathscr{P} = P_0$ is applied. For any given wavenumber and mean-flow speed U_m, the allowed values of the phase speed can be located from intersections between the plotted curve and a horizontal line drawn at a height which corresponds to the effective wall stiffness. If U_m is fixed, then a lowest possible line can be defined so as to represent the stiffness obtained when the wavenumber is taken to be equal to the critical wavenumber $\alpha_c = (\bar{K}/\bar{B})^{1/4}$. (Recall that α_c was identified as a key wall parameter in §4.1.) Consequently, we can investigate the sequence of behaviour that occurs as U_m is increased by examining intersections with horizontal lines of decreasing height. Changes in behaviour will first be realized for $\alpha = \alpha_c$. It can be seen that, provided U_m is not too large, there will be one intersection that represents an upstream wave and another that corresponds to a downstream wave. The onset of travelling wave flutter can be identified when the mean-flow speed is increased to a level that is sufficient to allow the downstream wave to achieve the phase speed $c = 1$. The appropriate point is labelled (i)^a in the figure. Similarly, divergence instability can set in when the initially upstream-travelling wave reverses its direction of propagation at point (ii)^a. Finally, the onset of flutter instability can be visualized in terms of horizontal lines lying below the minimum point (iii)^a of the plotted curve. In such cases, the absence of any intersections implies that there are no real-valued solutions for the phase speed. Instead, there is a pair of complex-conjugate solutions, one of which represents the flutter instability.

4.5.3. *Case when α_c and the Tollmien–Schlichting wavenumber are comparable*

So far, there is nothing new to report. We have merely given a different form of presentation to results discussed earlier. Curves (*b*) in figure 8 were determined by using the approximation $\mathscr{P} = P_d$. They plot the variation of the right-hand side of equation (83) when $\mathscr{P}$ is replaced by the quantity

$$P_d^r(\alpha, c) = P_0(c) + \frac{\alpha^2 \mathrm{Re}\,\{P_1(c)\}}{1 + \alpha^2 \mathrm{Re}\,\{I_1(c)\}}\,. \tag{84}$$

Thus, the effect of the critical layer, which is manifested in the imaginary parts of the functions P_1 and I_1, has been deliberately ignored. When P_d^r rather than P_0 is substituted for $\mathscr{P}$, the function on the right-hand side of the dispersion relation becomes dependent upon the wavenumber. As a consequence, our graphical analysis is now restricted to a single wavenumber, which for the particular case considered was set by taking $\alpha^2 = 1/2$. It can be seen that the form of the plot is altered significantly from that which was found when only the P_0-term was retained. There is a singularity in P_d^r, and hence in $mc^2 + P_d^r$, at a positive value of c. By considering intersections between curves (*b*) in figure 8 and horizontal lines, it may be concluded that for small enough flow speeds there are three, rather than two, possible values of the phase speed. In addition to the upstream and downstream solutions found before, there is a solution with a relatively small positive phase speed. As will be demonstrated later, this solution can be identified as the inviscid counterpart of a Tollmien–Schlichting wave. When the mean-flow speed is increased, the phase speed of the faster downstream wave decreases until it can take the value $c = 1$ at point (i)^b. Travelling wave flutter may then set in, just as before. However, the upstream wave can no longer change its direction of propagation. By considering point (iii)^b, it may be observed that the phase velocity can only vanish in the limit where the effective wall stiffness also vanishes, which would correspond to an infinite flow speed. Thus, there would not appear to be any possibility of divergence instability. (It should be noted that there is no physical interpretation for the parts of the plotted curve which lie below the x-axis, since the wall stiffness cannot be negative.) It can be seen that flutter instability is also excluded. Instead, the solution that corresponds to travelling wave flutter coalesces with the third solution corresponding to the Tollmien–Schlichting mode. Again, the existence of a minimum at point (iii)^b in the plotted curve indicates the occurrence of modal coalescence.

The account given immediately above may be brought into question. It could be considered inconsistent to neglect the effect of the critical layer when our stated aim is to examine the consequences of taking the rational approximation $\mathscr{P} = P_d$. If $\mathscr{P}$ is replaced by P_d, rather than the real-valued function P_d^r, then there is no longer any singularity for a real value of the phase speed. However, a residue of the singular behaviour can be traced in the extremely rapid variations that are displayed by both the real and the imaginary parts of P_d. These occur over a very small range of phase speeds, centred around the value at which P_d^r was found to be singular. Rather than attempting to provide a more formal justification for the graphical analysis which employed the quantity P_d^r, we will simply check that such an analysis does, in fact, predict the correct behaviour for solutions of the inviscid dispersion relation in the case where the unamended rational approximation $\mathscr{P} = P_d$ is applied. Such solutions are displayed in figure 9. The real and imaginary parts of the phase velocity are plotted for a wavenumber fixed at the critical value α_c. In order to facilitate comparisons with solutions computed from the Orr–Sommerfeld

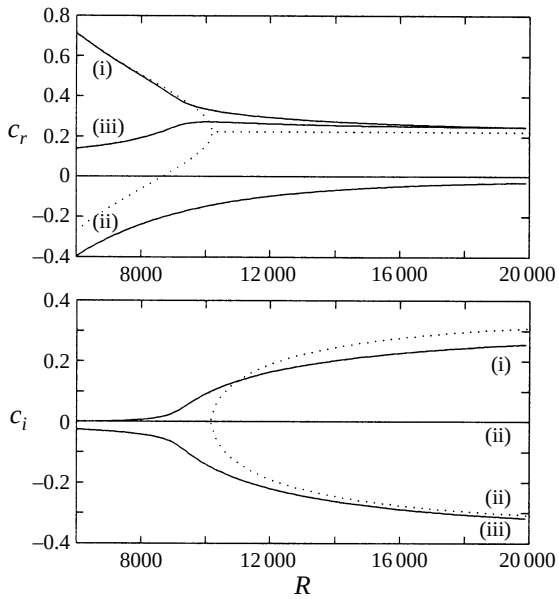

FIGURE 9. Real and imaginary parts of the phase velocity, as obtained from the inviscid dispersion relation using the approximations $\mathscr{P} = P_d$ (solid lines) and $\mathscr{P} = P_0$ (dotted lines). The non-dimensional wall parameters are $m = 2$, $B = 4 \times 10^7$, $K = 1 \times 10^7$, $T = d = 0$. The wavenumber is held constant at the critical value $\alpha = \alpha_c$, where $\alpha_c = (K/B)^{1/4} = 1/\sqrt{2}$. The labels (i), (ii) distinguish the two solution branches that are related to the free waves that would propagate in opposite directions along the compliant wall in the absence of the fluid. The solution marked (iii) can be associated with the Tollmien–Schlichting mode of instability. (In the case where $\mathscr{P} = P_d$, the imaginary part of the phase velocity is identically zero for the branch of solutions that represents an upstream-travelling wave.)

equation, the variation is shown with respect to the Reynolds number R, rather than the mean-flow speed U_m. Plots are also given for solutions that were obtained using the lowest-order approximation $\mathscr{P} = P_0$. As expected, there are three distinct solution branches when P_d is substituted for $\mathscr{P}$. The solution with the largest positive phase speed corresponds to travelling wave flutter. It can be seen that for sufficiently large Reynolds numbers, this solution is highly unstable. By contrast, the other solution representing a wave with a downstream phase speed is subject to strong stabilization. From a comparison with the results obtained using the lowest-order approximation, it becomes apparent that the merger that would have led to flutter instability has been supplanted. Finally, it may be noted that when the approximation $\mathscr{P} = P_d$ is applied, there is a solution that always represents an upstream travelling wave. Taken together, the above observations provide a vindication for the results that were obtained, more simply, using the graphical analysis.

Figure 10 displays numerical solutions of the Orr–Sommerfeld equation for the same values of the wall parameters and the wavenumber as were considered in the previous figure. For ease of comparison, there is also a replot of the solutions obtained from the inviscid shear layer theory by substituting P_d for $\mathscr{P}$. It can be seen that the more sophisticated version of the inviscid dispersion relation gives a fairly reliable guide to the behaviour discovered by solving the Orr–Sommerfeld equation directly. In particular, the inviscid theory anticipates, correctly, the existence of an additional branch of solutions with a downstream phase speed. It is a straightforward

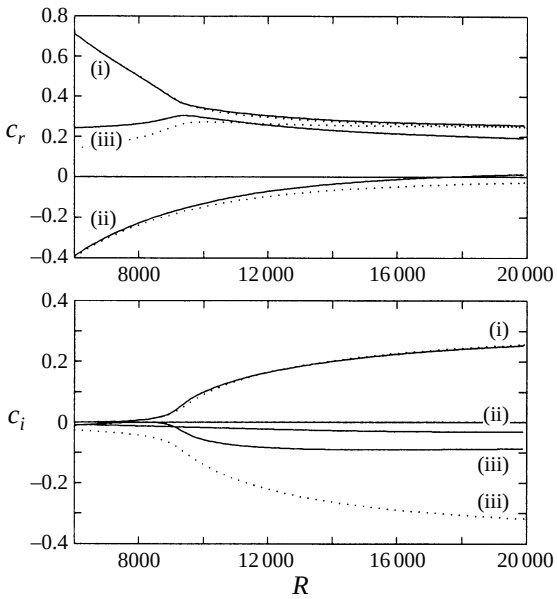

FIGURE 10. Real and imaginary parts of the phase velocity, as obtained from direct numerical solution of the Orr–Sommerfeld equation (solid lines) and the inviscid dispersion relation using the approximation $\mathscr{P} = P_d$ (dotted lines). The non-dimensional wall parameters and the fixed wavenumber are the same as in figure 9.

matter to verify that such solutions represent Tollmien–Schlichting waves when they are obtained directly from the Orr–Sommerfeld equation. The inviscid theory also predicts the interaction between travelling wave flutter and what we have now identified as the Tollmien–Schlichting mode. As a consequence of this interaction, travelling wave flutter becomes very strongly unstable. Simultaneously, the Tollmien–Schlichting mode is subjected to a stabilization which, though not so strong as the destabilization suffered by travelling wave flutter, is still considerable. Thus, the interaction retains the hallmarks of a Class A/Class B modal coalescence. The Class-C character of the subsequent instability is confirmed by the fact that the temporal growth rates are little affected by the introduction of moderate levels of damping. As might have been expected, the inviscid shear layer theory gives quite poor quantitative predictions for the real and imaginary parts of the phase speed along the solution branch associated with Tollmien–Schlichting waves. A more accurate treatment would require a careful account of the balance between the viscous effects attributable to the critical layer and those which arise from the viscous wall layer. However, it can be seen that such a treatment is not necessary if we are only interested in locating the onset of the strong instability arising when the Tollmien–Schlichting mode interacts with travelling wave flutter. In fact, if we return to the graphical analysis presented earlier, which involved the neglect of all critical layer effects, it may be conjectured that viscosity is inessential to the mechanism of interaction and coalescence, except in so far as there would appear to be a need for a shear flow.

We now turn to the branch of solutions that in the inviscid theory, subject to the approximation $\mathscr{P} = P_d$, was always found to represent an upstream-travelling wave. For the corresponding solutions obtained directly from the Orr–Sommerfeld equation, there is a reversal in the direction of wave propagation for high enough Reynolds numbers. By making a comparison between the appropriate plots in figures 9 and 10

it can be seen that the Reynolds number at which there is a wave with a vanishing phase speed is about twice the critical Reynolds number predicted for the onset of divergence instability using the inviscid approximation $\mathscr{P} = P_0$. It may also be observed that the solutions derived from the Orr–Sommerfeld equation have an appreciable negative growth rate. Further investigation revealed that the introduction of fairly high levels of wall damping do not lead to instability for Reynolds numbers close to that at which the phase speed changes sign. Finally, it should be noted that although the inviscid theory, with the rational approximation $\mathscr{P} = P_d$, fails to anticipate the reversal in phase speed discovered from the numerical solution of the Orr–Sommerfeld equation, the predictions for the behaviour of the upstream-travelling waves are still considerably better than those that were obtained using the lowest-order inviscid approximation. Further improvements can be made if a viscous-wall-layer correction is included (but there is the complication that, for negative phase speeds, an appropriate branch of the square root needs to be taken for the quantity $\mathscr{P}_v$ defined in (68)). In particular, it is possible to obtain some measure of agreement for the growth rates of the upstream waves. As a consequence, it would seem plausible to attribute the stability noted in the solutions of the Orr–Sommerfeld equation to the effect of the viscous-wall-layer. The incorporation of a viscous wall layer correction also leads to a slight improvement in the values predicted for the real parts of the phase speeds. However, it is still not possible to locate the appearance of a wave with a vanishing phase speed.

4.5.4. *Case when α_c is much smaller than the Tollmien–Schlichting wavenumber*

It may have been noticed that the suppression of the divergence instability seems to be somewhat at odds with results presented in §4.4. For the case of a compliant wall modelled as a tensioned membrane, solution of the Orr–Sommerfeld equation revealed the onset of divergence instability at the precise critical Reynolds number that could be derived using the inviscid dispersion relation in conjunction with the simplest approximation $\mathscr{P} = P_0$. The success of the lowest-order predictions, in this particular case, stems from the fact that there is no specific lengthscale associated with the motion of a tensioned membrane. The effective wall stiffness is independent of the wavenumber, and so remains finite as the wavenumber approaches zero, where the instability was found to set in. (A discussion of the behaviour of the function P_d for vanishing wavenumbers is included in Appendix B.) By contrast, for Kramer-type compliant surfaces there will always be a critical wavenumber at which the wall stiffness is minimized. In the analysis presented immediately above, we assumed, implicitly, that the critical wavenumber was comparable to wavenumbers typical of the Tollmien–Schlichting instability. Such an assumption of similar lengthscales is necessary in order to obtain optimized stability effects for Tollmien–Schlichting waves. If, on the other hand, we had chosen a compliant wall with a critical wavenumber very much smaller than the wavenumbers typical of unstable Tollmien–Schlichting waves, we might have anticipated only limited departures from the simple form of behaviour found by setting $\mathscr{P} = P_0$. Singularities attributable to the Tollmien–Schlichting mode would no longer be expected to have any significant influence on the character of the flow-induced surface waves.

This expectation was borne out by the results obtained from a more detailed investigation. When the wall parameters were selected to give the critical wavenumber as $\alpha_c = 1/16$, it was found that the introduction of a small amount of wall damping led to the destabilization of divergence in the exact manner predicted using the lowest-order inviscid approximation. Figure 11 displays the neutral stability curve for

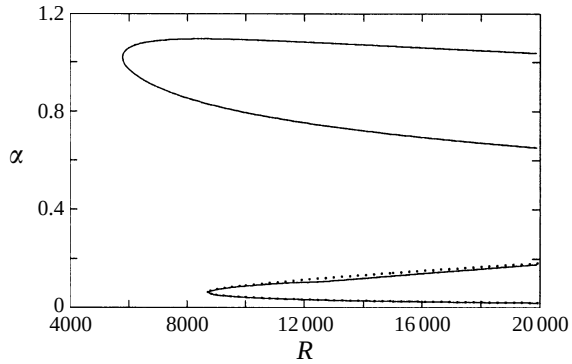

FIGURE 11. Neutral stability curves as obtained from direct numerical solution of the Orr–Sommerfeld equation (solid lines) and the inviscid dispersion relation using the approximation $\mathscr{P} = P_0 + \alpha^2 \mathrm{Im}(P_1)$ (dotted line). The uppermost of the neutral curves corresponds to the Tollmien–Schlichting instability. Divergence is found at the lower wavenumbers. The non-dimensional wall parameters are $m = 2$, $B = 5.12 \times 10^9$, $K = 7.8125 \times 10^4$, $T = 0$, $d = 200$.

divergence computed by solving the Orr–Sommerfeld equation directly, together with the corresponding curve determined from the inviscid theory when $\mathscr{P}$ is replaced by $P_0 + \alpha^2 \mathrm{Im}(P_1)$. It can be seen that there is good agreement between the two curves. (The $O(\alpha^2)$ phase shift due to the critical layer was incorporated in order to allow for the possibility of travelling wave flutter instability. In practice, the effect of the critical layer was found to be insignificant for the small wavenumbers involved: very slight wall damping was sufficient to stabilize travelling-wave-flutter over the range of Reynolds numbers considered.) The figure also includes the neutral stability curve for the Tollmien–Schlichting mode. This is little changed from the curve that would be found for the case of rigid walls. The wavenumbers concerned are well removed from the critical wavenumber, so the effective wall stiffness remains much larger than its allowed minimum. Figure 12 shows the variation, with the Reynolds number, of the real and imaginary parts of the phase speed for solutions fixed at the critical wavenumber. In addition to the plot for the branch of solutions corresponding to divergence instability, there is a plot for the branch that, had the critical layer effects been stronger, would have led to travelling-wave-flutter instability. It can be observed that the results derived using the inviscid theory are indistinguishable from those obtained by solving the Orr–Sommerfeld equation numerically. It may also be noted that, shortly after the phase speed reversal which marks the onset of divergence instability, there is a modal interaction that causes the associated branch of solutions to become more strongly unstable. Simultaneously, the branch of solutions that is already stabilized by the wall damping is subjected to a further stabilization. Thus, the interaction between the two modes bears the hallmarks of the flutter instability, as can be confirmed by comparing the results displayed in figure 12 with the results derived from the lowest-order inviscid approximation that were presented earlier in figure 9. From such a comparison it can be inferred that the presence of wall damping has caused the divergence and flutter instabilities to become continuously connected. The onset of flutter instability no longer occurs in an abrupt manner. As a final observation we note that the group velocity vanishes at the point in the (R, α)-plane where divergence instability first sets in. This suggests that divergence will take the form of an absolute instability.

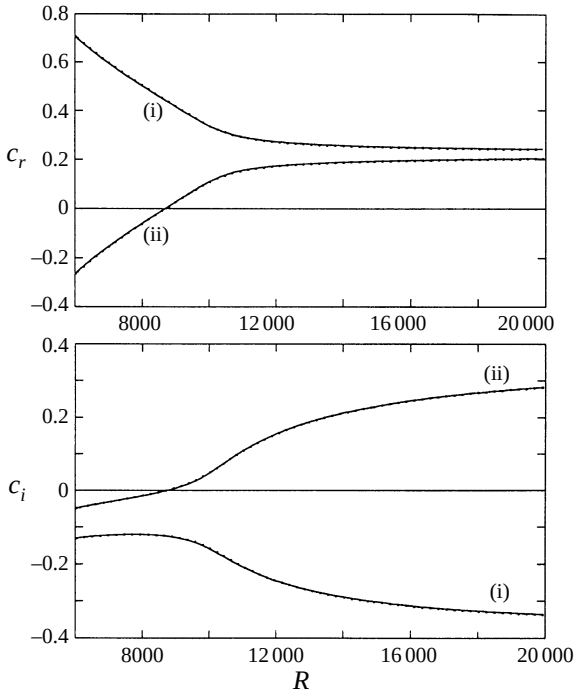

FIGURE 12. Real and imaginary parts of the phase velocity, as obtained from direct numerical solution of the Orr–Sommerfeld equation (solid lines) and the inviscid dispersion relation using the approximation $\mathscr{P} = P_0 + \alpha^2 \mathrm{Im}(P_1)$ (dotted lines). The non-dimensional wall parameters are the same as in figure 11. The wavenumber is held constant at the critical value $\alpha = \alpha_c$, where $\alpha_c = (K/B)^{1/4} = 1/16$.

5. Conclusions

We have investigated the stability of plane channel flow between compliant walls. The present study has been restricted to disturbances which have the same symmetry, with respect to the channel centreline, as the Tollmien–Schlichting mode of instability. In addition to documenting the well-known stabilizing effect of wall compliance on Tollmien–Schlichting waves, we have examined the behaviour of the flow-induced surface instabilities that, in practical applications, would limit the potential for obtaining a transition delay. The flow-induced surface instabilities were investigated using a dispersion relation derived from an inviscid shear layer theory. The effects of the viscous wall layer could be ascertained by implementing a simple modification to the inviscid dispersion relation. Results obtained using various analytic approximations to the dispersion relation were compared with the results obtained from the direct numerical solution of the Orr–Sommerfeld equation. As with previous studies for the case of Blasius flow, various forms of flow-induced surface instability could be identified. These included the divergence and travelling-wave-flutter instabilities, as well as the flutter instability arising from their modal coalescence. It was shown that the branch of solutions associated with the travelling-wave-flutter instability could also interact with the branch representing Tollmien–Schlichting waves. In such circumstances the Tollmien–Schlichting mode could take on an inviscid character.

The instability most easily described using the inviscid theory as a starting point is travelling wave flutter. This arises when there is a critical layer to generate a phase

shift between the wall velocity and the perturbation fluid pressure at the wall. The characteristics of the instability classified as divergence proved to be more difficult to determine. However, though the results concerning the onset of divergence instability remain somewhat incomplete, they represent definite progress over previous studies based on Blasius flow. Such studies, which relied upon a potential theory model of the mean flow, achieved very limited success in linking analytic results for the onset of divergence with numerical solutions of the Orr–Sommerfeld equation. (For a recent example, reference should be made to figure 17 in Carpenter & Morris 1990.) Moreover, potential-flow modelling often yields poor predictions for the critical flow speeds found in experiments (Riley *et al.* 1988). It is likely that the difficulties encountered in predicting the onset of divergence instability for the case of Blasius flow can be traced to the same source as was found for channel flow. For Blasius flow, we should again expect to find singularities in the function defining the ratio of the wall pressure to the wall displacement. These would be attributable to the Tollmien–Schlichting waves that can propagate along a Blasius boundary layer adjacent to a rigid wall. Thus, for Blasius flow as well as for plane channel flow, it may not always be feasible to give an account of flow-induced surface waves without also treating Tollmien–Schlichting waves, or their inviscid counterparts, within the same analytic framework.

What are, perhaps, the most significant results depend on how the wavenumber, α_c, of the slowest free wave on the compliant wall compares in magnitude with the wavenumber, α_{ts}, of the most unstable Tollmien–Schlichting wave. For those compliant walls which are effective at stabilizing the Tollmien–Schlichting waves, the two wavenumbers tend to be comparable in magnitude. For such walls it seems unlikely that divergence will exist as an instability when the flow is laminar. It appears to be replaced by a strong interaction between the Tollmien–Schlichting waves and travelling wave flutter. Viscous and wall-damping effects are not essential for this process, but damping does appear to be required for full modal coalescence. For cases where $\alpha_c \ll \alpha_{ts}$, including special cases like the tensioned membrane, divergence does exist as an instability. Strong interaction and coalescence are now possible between the divergence and travelling-wave-flutter eigenmodes, leading to zero group velocity and, presumably, absolute instability.

These conclusions probably carry over to the Blasius boundary layer. The limited evidence available from previous theoretical studies and recent numerical simulations (Lucey *et al.* 1996) suggests that divergence does not occur when α_c and α_{ts} are comparable in magnitude. Since this is precisely the case of interest for laminar-flow control, it is a highly significant result. Previous studies of the optimization of compliant walls for transition delay were based on estimates of divergence onset taken from potential-flow theory. This now appears highly conservative and it may well be possible to suppress Tollmien–Schlichting waves completely using multiple-panel compliant walls irrespective of how high the Reynolds numbers become (Carpenter 1993, 1994; Davies & Carpenter 1997).

Appendix A. Exact solutions of Rayleigh's equation

For the parabolic mean flow profile $U = 1 - y^2$, and for a disturbance with phase velocity $c = 1$, Rayleigh's equation takes the simple form

$$-y^2\left(\mathrm{D}^2 - \alpha^2\right)\phi + 2\phi = 0\,, \tag{A 1}$$

where α is the wavenumber and $\phi(y)$ is the disturbance profile. It may be verified that this has an exact symmetric solution

$$\Phi(y) = \cosh(\alpha y) - \frac{\sinh(\alpha y)}{\alpha y} \,. \tag{A 2}$$

Using the definition of $\mathscr{P}$ in the form stated in equation (60) we may then obtain the result that

$$\mathscr{P}(\alpha, 1) = \frac{1}{\alpha \coth \alpha - 1} - \frac{3}{\alpha^2} \,. \tag{A 3}$$

It is straightforward to check that this can be written as

$$\mathscr{P}(\alpha, 1) = \frac{1}{5}\left(\frac{1 + \frac{1}{14}\alpha^2 + \cdots}{1 + \frac{1}{10}\alpha^2 + \cdots}\right), \tag{A 4}$$

which conforms with the expression (82) that was noted in connection with the rational approximation $\mathscr{P} = P_d$. It is also easy to establish that

$$0 < \mathscr{P}(\alpha, 1) \leqslant \mathscr{P}(0, 1) = \tfrac{1}{5} \,. \tag{A 5}$$

Retracing the steps involved in developing the inviscid theory, it may then be shown that the use of a long-wavelength approximation can only lead to an underestimation of the critical flow velocity for the onset of travelling wave flutter.

Rayleigh's equation for $c = 1$ also has the exact antisymmetric solution

$$\Phi^{as}(y) = \sinh(\alpha y) - \frac{\cosh(\alpha y)}{\alpha y} \,. \tag{A 6}$$

This has a $1/y$ singularity at the channel centre $y = 0$. Thus we can anticipate greater difficulty in developing the inviscid theory for any antisymmetric form of travelling wave flutter. (The case where $0 < c < 1$ and $\alpha = 0$ has been considered by Huang 1997.)

Appendix B. A note on the behaviour of the function P_d in the limit where both the wavenumber and the phase velocity vanish

The behaviour displayed by the approximating function $P_d(\alpha, c)$ when $(\alpha, c) \to (0, 0)$ is pertinent to the onset of divergence instability in the case where the compliant wall is modelled as a tensioned membrane. Solution of the Orr–Sommerfeld equation indicates that instability sets in when both the wavenumber and the phase velocity vanish. The behaviour in the same limit would also be expected to be significant for a Kramer-type compliant surface when the wall parameters are chosen so as to yield a very small value for the critical wavenumber, i.e. the wavenumber at which the effective wall stiffness is minimized.

If we consider the definition of P_d given by (80), then we can obtain the result

$$\lim_{\alpha \to 0} P_d(\alpha, c) = P_0(c) \tag{B 1}$$

for non-vanishing values of the phase velocity. Proceeding to take the limit as the phase velocity tends to zero, it may be seen that

$$\lim_{c \to 0}\left(\lim_{\alpha \to 0} P_d(\alpha, c)\right) = P_0(0) = \tfrac{8}{15} \,. \tag{B 2}$$

By contrast, if we first allow the phase velocity to approach zero, and then consider

the limit of a vanishing wavenumber, we obtain (compare equation (81))

$$\lim_{\alpha\to 0}\left(\lim_{c\to 0} P_d(\alpha, c)\right) = 0\,. \tag{B 3}$$

Thus the function P_d displays a discontinuity at the point $(\alpha, c) = (0, 0)$. Without embarking upon a more elaborate investigation, it would be impossible to determine the appropriate form of limiting behaviour. However, since for the case of a tensioned membrane a perturbation analysis based upon the approximation $\mathscr{P} = P_0$ was found to yield the correct prediction for the onset of divergence instability, it would appear that (B 2), rather than (B 3), should be employed.

REFERENCES

Benjamin, T. B. 1960 Effects of a flexible surface on hydrodynamic stability. *J. Fluid Mech.* **9**, 513–532.

Benjamin, T. B. 1963 The threefold classification of unstable disturbances in flexible surface bounding inviscid flows. *J. Fluid Mech.* **16**, 436–450.

Bridges, T. J. & Morris, P. J. 1984 Differential eigenvalue problems in which the parameter appears nonlinearly. *J. Comput. Phys.* **55**, 437–460.

Briggs, R. J. 1964 *Electron–Stream Interaction with Plasmas.* MIT Press.

Canuto, C., Hussaini, M. Y. , Quarteroni, A. & Zang, T. A. 1988 *Spectral Methods in Fluid Dynamics.* Springer.

Carpenter, P. W. 1987 The optimization of compliant surfaces for transition delay. In *Proc. IUTAM Symp on Turbulence Management and Relaminarisation, Bangalore, India* (ed. H. W. Liepmann & R. Narasimha), pp. 305–313. Springer.

Carpenter, P. W. 1990 Status of transition delay using compliant walls. In *Viscous Drag Reduction in Boundary Layers* (ed. D. M. Bushnell & J. N. Hefner), pp. 79–113. AIAA.

Carpenter, P. W. 1993 The optimization of multiple-panel compliant walls for delay of laminar-turbulent transition. *AIAA J.* **31**, 1187–1188.

Carpenter, P. W. 1994 Can boundary-layer turbulence be eliminated without the use of auxiliary power? In *Proc. Flow Acoustics: A Technology Audit, Ecole Centrale de Lyon, France, 11–13 July*, pp. 84–86.

Carpenter, P. W. & Gajjar, J. S. B. 1990 A general theory for two- and three-dimensional wall-mode instabilities in boundary layers over isotropic and anisotropic compliant walls. *Theor. Comput. Fluid Dyn.* **1**, 349–378.

Carpenter, P. W. & Garrad, A. D. 1985 The hydrodynamic stability of flow over Kramer-type compliant surfaces. Part 1. Tollmien–Schlichting instabilities. *J. Fluid Mech.* **155**, 465–510.

Carpenter, P. W. & Garrad, A. D. 1986 The hydrodynamic stability of flow over Kramer-type compliant surfaces. Part 2. Flow-induced surface instabilities. *J. Fluid Mech.* **170**, 199–232.

Carpenter, P. W., Gaster, M. & Willis, G. J. K. 1983 A numerical investigation into boundary layer stability on compliant surfaces. In *Numerical Methods in Laminar and Turbulent Flow*, pp. 166–172. Pineridge.

Carpenter, P. W. & Morris, P. J. 1990 The effect of anisotropic wall compliance on boundary–layer stability and transition. *J. Fluid Mech.* **218**, 171–223.

Davies, C. 1995 Evolution of Tollmien-Schlichting waves over a compliant panel. PhD thesis, University of Warwick.

Davies, C. & Carpenter, P. W. 1997 Numerical simulation of the evolution of Tollmien–Schlichting waves over finite compliant panels. *J. Fluid Mech.* **335**, 361–392.

Drazin, P. G. & Reid, W. H. 1981 *Hydrodynamic Stability.* Cambridge University Press.

Ehrenstein, U. & Rossi M. 1993 Nonlinear Tollmien-Schlichting waves for plane Poiseuille flow with compliant walls. *Eur. J. Mech.* B/*Fluids* **12**, 789–810.

Gad-el-Hak, M., Blackwelder, R. F. & Riley, J. J. 1984 On the interaction of compliant coatings with boundary-layer flows. *J. Fluid Mech.* **140**, 257–280.

Gajjar, J. S. B. & Sibanda, P. 1996 The hydrodynamic stability of channel flow with compliant boundaries. *Theor. Comput. Fluid Dyn.* **8**, 105–129.

Ganiev, R. F., Ukrainskii, L. E. & Ustenko, I. G. 1988 Stabilisation of small perturbations of Poiseuille flow in a channel with elastic walls. *Izv. Akad. Nauk SSSR, Mekh. Zhid. i Gaza* **23**, 378–382.

Gaster, M. 1965 On the generation of spatially growing waves in a boundary layer. *J. Fluid Mech.* **22**, 433–441.

Green, C. H. & Ellen, C. H. 1972 The stability of plane Poiseuille flow between flexible walls. *J. Fluid Mech.* **51**, 403–416.

Grotberg, J. B. 1994 Pulmonary flow and transport phenomena. *Ann. Rev. Fluid Mech.* **26**, 529–571.

Grotberg, J. B. & Davis, S. H. 1980 Fluid dynamic flapping of a collapsible channel: sound generation and flow limitation. *J. Biomech.* **13**, 219–230.

Grotberg, J. B. & Reiss, E. L. 1984 Subsonic flapping flutter. *J. Sound Vib.* **92**, 349–361.

Grotberg, J. B. & Shee, T. R. 1995 Compressible-flow channel flutter. *J. Fluid Mech.* **159**, 175–193.

Hains, F. D. & Price, J. F. 1962 Effect of a flexible wall on the stability of Poiseuille flow. *Phys. Fluids* **5**, 365.

Healey J. J. 1995 On the neutral curve of the flat-plate boundary layer: comparison between experiment, Orr–Sommerfeld theory and asymptotic theory. *J. Fluid Mech.* **288**, 59–73.

Heisenberg, W. 1924 Über Stabilität und Turbulenz von Flussigkeitsströmen. *Ann. Physik (4)* **74**, 577–627.

Huang, L. 1997 Reversal of the Bernoulli effect and channel flutter. *J. Fluids Structures* (submitted).

Kamm, R. D. & Pedley, T. J. 1989 Flow in collapsible tubes: a brief review. *J. Biomech. Engng* **111**, 177–179.

Korotkin, A. I. 1965 The stability of plane Poiseuille flow in the presence of elastic boundaries. *Prikl. Mat. Mekh.* **29**, 1122–1127.

Landahl, M. T. 1962 On the stability of a laminar incompressible boundary over a flexible surface. *J. Fluid Mech.* **13**, 609–632.

Lucey, A. D., Cafolla, G. J. & Carpenter, P. W. 1996 A numerical simulation of a boundary-layer flow interacting with a passive compliant boundary. In *Proc. 15th Intl Conf. on Numerical Meths. in Fluid Dynamics, 24–28 June, Monterey, CA*.

Lucey, A. D. & Carpenter, P. W. 1995 Boundary layers instability over compliant walls: Comparison between theory and experiment. *Phys. Fluids* **7**, 2355–2363.

Luo, X. Y. & Pedley, T. J. 1996 A numerical simulation of unsteady flow in a two-dimensional collapsible channel. *J. Fluid Mech.* **314**, 191–226.

Miles, J. W. 1957 On the generation of surface waves by shear flows. *J. Fluid Mech.* **3**, 185–199.

Pierce, R. 1992 The Ginzburg-Landau equation for interfacial instabilities. *Phys. Fluids* A **4**, 2486–2494.

Riley, J. J., Gad-el-Hak, M. & Metcalfe, R. W. 1988 Compliant coatings. *Ann. Rev. Fluid Mech.* **20**, 393–420.

Rossi, M. 1991 Nonlinear longwave shortwave coupling in flow over a compliant surface. *European J. Mech.* B/*Fluids* **10**, 159–164.

Rotenberry, J. M. 1992 Finite amplitude shear waves in a channel with compliant boundaries. *Phys. Fluids* A **4**, 270–276.

Rotenberry, J. M. & Saffman, P. G. 1990 Effect of compliant boundaries on weakly nonlinear shear waves in channel flow. *SIAM J. Appl. Maths* **50**, 361–394.

Sen, P. K. & Arora, D. S. 1988 On the stability of laminar boundary-layer flow over a flat plate with a compliant surface. *J. Fluid Mech.* **197**, 201–240.

Tsvelodub, O. Yu. 1977 Stability of plane Poiseuille flow in an elastic channel. *Zh. Prikl. Mekh. Tekh. Fiz.* **5**, 75–80.

Weaver, D. S. & Paidoussis, M. P. 1977 On collapse and flutter phenomena in thin tubes conveying fluid. *J. Sound Vib.* **50**, 117–132.

Willis, G. J. K. 1986 Hydrodynamic stability of boundary layers over compliant surfaces. PhD thesis, University of Exeter.

Yeo, K. S., Khoo, B. C. & Zhao, H.Z. 1996 The absolute instability of boundary-layer flow over visocelastic walls. *Theor. Comput. Fluid Dyn.* **8**, 237–252.